

Mid-UV Determination of Elliptical Galaxy Abundances and Ages

Jennifer M. Lotz¹

Johns Hopkins University, 3400 N. Charles St., Baltimore, MD 21218

Henry C. Ferguson² and Ralph C. Bohlin³

Space Telescope Science Institute, 3700 San Martin Drive, Baltimore, MD 21218

accepted by the Astrophysical Journal

ABSTRACT

We investigate the effects of abundance and age on the mid-UV spectra and Mg_2 strengths of stellar populations using simple population synthesis models. These models are used to constrain the star formation history of four nearby elliptical galaxies and spiral bulges. The mid-UV (1800 - 3200 Å) light of evolved stellar populations (> 1 Gyr) is dominated by the main sequence turn-off, unlike the optical light which is dominated by the red giant branch. Because the main sequence turn-off is sensitive to age and metallicity in ways different from the RGB, a detailed investigation of the mid-UV features of elliptical galaxies may help break the age-metallicity degeneracy that plagues optical techniques. Also, a better understanding of this wavelength region is useful for the studies of $0.5 \leq z \leq 1.5$ galaxies for which the rest frame mid-UV is redshifted into the visible. We create simple, single age (3-20 Gyr), single metallicity ($Z = 0.0004 - 0.05$) spectral energy distributions (SEDs) extending into the UV using the Kurucz model stellar fluxes. Comparison to standard stars' mid-UV spectra reveals that the Kurucz model fluxes accurately model a blend feature of FeI and MgI at 2538 Å (B12538) and the slope of the continuum between 2600 and 3100 Å (S2850). We find that our simple single age, single metallicity SEDs agree well with these mid-UV features of globular clusters. However, the majority of the galaxies do not agree with the B12538, S2850, and Mg_2 values given by these simple models. The mid-UV features appear to require both an old metal-rich and an old metal-poor ($Z \leq 0.001$) population. The implied metal-poor population is less than 10% of the total mass for all the galaxies but dominates the SEDs shortward of 3000 Å. Intermediate age (1-5 Gyr) populations are not required to match the UV for any of the galaxies, but are not ruled out. Despite being limited by the quality of the model stellar fluxes, our study has yielded two promising mid-UV spectral diagnostics (B12538 and S2850) and suggests unique and complex star formation histories for elliptical galaxies.

Subject headings: galaxies: abundances – galaxies: elliptical and lenticular, cD – galaxies: evolution – galaxies: stellar content – ultraviolet: galaxies

1. Introduction

The integrated light of elliptical galaxies contains many clues to their star formation histories. Currently, the most popular approach to decipher-

ing the broad band colors and spectral features of elliptical galaxies and star clusters is evolutionary population synthesis (Charlot & Bruzual 1991; Bressan, Chiosi, & Fagotto 1994; Worthey 1994). This technique models the integrated light for a stellar population of a given age and metallicity by summing up the light from individual stars along theoretical isochrones. The resulting spectral energy distribution (SED) is dependent

¹jlotz@pha.jhu.edu

²ferguson@stsci.edu

³bohlin@stsci.edu

on the libraries of stellar evolutionary tracks and stellar fluxes, the chosen star formation rate and initial mass function (IMF), and in the case of multi-metallicity populations, the chemical enrichment history. Charlot, Worthey, & Bressan (1996) examined the differences between several recent models and found that they are seriously limited by the dearth of reliable libraries for cool and non-solar composition stars and by the uncertain properties of post main sequence stars. Nevertheless, population synthesis is appealing because of its ability to prescribe a fundamental recipe for a galaxy.

Attempts to unravel the history of star formation in elliptical galaxies via spectral synthesis are plagued by the “age-metallicity degeneracy” (Worthey 1994 and references therein). The effective temperature of the red giant branch (RGB) decreases with increasing age and metallicity in such a way that the RGB of an old solar metallicity population looks nearly identical to that of a more metal-rich, slightly younger population. Because the RGB dominates both the integrated line strength and broad band color longward of 4000 Å, a degeneracy of these properties in age and abundance results for stellar populations older than 1 Gyr. The most promising attempts to disentangle age and metallicity from integrated spectra have involved use of the Balmer absorption lines (Gonzalez 1993; Greggio 1997) and mid-UV colors (Dorman, O’Connell, & Rood 1995). All of these methods rely on spectral diagnostics for which the main sequence begins to dominate over the RGB.

The contribution of the main sequence turn-off to the integrated light is greatest in the mid-UV region ($\sim 2500\text{-}3500$ Å); the contribution of the far-UV bright HB and post HB stars to the integrated light is less than 50% at 2500 Å (Worthey, Dorman, & Jones 1996). Heap et al. (1998) suggest that the spectral break at 2900 Å is correlated with spectral type of the turn-off population but weakly influenced by metallicity. Also, the continuum of mid-UV is affected by the metallicity of the stellar population. Dorman et al. (1995) found that the color (2500-V) was correlated with metallicity and Fanelli et al. (1990, 1992) found δ (2600-V) 10 times more sensitive to [Fe/H] than δ (B-V). Because the spectral type of the main sequence turn-off stars dominates the absorption features of the mid-UV and the continuum is highly sensitive

to chemical content, a detailed investigation of the integrated mid-UV light of stellar populations may help break the age-metallicity degeneracy.

One observational result population synthesis models have sought to explain is the correlation between the “UV upturn” shortward of 2000 Å and the optical Mg₂ absorption line strength in elliptical galaxies (Worthey 1994; Dorman et al. 1995; Bressan et al. 1994). The brightest galaxies in UV also have the strongest Mg₂ absorption (Burstein et al. 1988), suggesting that these UV strong galaxies are metal-rich and possibly enhanced in α element abundances. In the most metal-rich galaxies, the primary source of far-UV emission appears to be extreme horizontal branch (EHB) stars and their descendants, the AGB-manqué stars. While the bulk of the evidence favors a metal-rich origin for the EHB stars (Dorman et al. 1995; Brown et al. 1997), models with a distribution of metallicities including a metal-poor tail (Park & Lee 1997) cannot be excluded. In any case, the models for hot populations are strongly dependent on mass loss on the red giant branch and on the helium abundance. Small changes in these two parameters can give wildly different UV upturns at fixed age and metallicity. For the purposes of this paper, the UV upturn is simply an underlying continuum that must be subtracted from the galaxy spectra prior to analysis of the spectral features.

The star formation history of nearby ellipticals, particularly M32, has been in the subject of much debate. In 1980, O’Connell (1980) proposed that a 5 Gyr stellar sub-population is responsible for the relatively blue $B - V$ color of M32. The idea that M32 contains a large intermediate age population was supported by detailed comparison of M32 and 47 Tuc (an old “metal-rich” globular cluster) near UV spectra (3800 - 4400 Å) (Rose 1994). The study of H β and H γ absorption lines, which are dependent on the main sequence turn-off stars in old stellar populations, suggest intermediate ages for many ellipticals (Gonzalez 1993; Greggio 1997). However, recent HST observations of M32’s red giant branch implies that at least half of M32’s stars are older than 8 Gyr (Grillmair et al. 1996). The metallicity distribution of M32 and other ellipticals has also been investigated. Rose & Deng (1999) found evidence for a hot metal-poor population in an otherwise metal-rich

population in the mid-UV spectra of M32. The width of M32's RGB requires that the stars span a substantial range in metallicity (Grillmair et al. 1996). The estimated metallicity distribution has a low metallicity tail extending down to $[\text{Fe}/\text{H}] = -1.5$ but is strongly skewed to solar metallicity and is much narrower than expected from a closed box chemical enrichment scenario. Comparisons to synthetic spectra suggest that other galaxies, including NGC 1404, NGC 4649, and the bulge of M31, also show a deficit of low metallicity stars relative to closed box models (Bressan et al. 1994; Worthey et al. 1996).

The ages of distant elliptical galaxies has been the subject of some debate as well. Spinrad et al. (1997) determined an age of ~ 3.5 Gyr (assuming a solar metallicity) for LBDS 53W091 ($z \sim 1.55$) by comparing the rest frame mid-UV spectral features to solar metallicity F and G stars and population synthesis models. A galaxy this old at a redshift of 1.55 would rule out a $H_0 > 50$, $\Lambda = 0$, $\Omega = 1$ universe. A later comparison of this galaxy's spectra to improved F star models gave an age of 1-2 Gyr (assuming $Z \geq Z_\odot$), relaxing the cosmological constraints (Heap et al. 1998). Because galaxies with $0.5 \leq z \leq 1.5$ have their mid-UV spectra redshifted into the visible range, a better understanding of the mid-UV features of old stellar populations will be useful for dating distant galaxies.

Using simple population synthesis models, we examine the mid-UV features and Mg_2 strengths of four nearby elliptical galaxies and spiral bulges. In order to study the spectral properties of the underlying main sequence and RGB branch stars, we exclude the uncertain hot HB and post HB stars from our models' isochrones and attempt to subtract out the far-UV component from the galaxies' spectra. Specifically we use the blend feature at 2538 Å (B12538) and Mg_2 line indices and introduce a new tool for examining the mid-UV continua, the slope between 2600 and 3100 Å ($S2850$), to determine the galactic properties. The investigation of the mid-UV dependence on age and abundance via population synthesis is severely limited by inaccuracies in our model stellar fluxes. However, B12538 and $S2850$ appear to be adequately modeled by the Kurucz fluxes. We find for our simple population models that populations older than 3 Gyr separate out in the $S2850$

v. B12538 and $S2850$ v. Mg_2 planes. Although globular cluster spectra agree with simple, single metallicity, single age populations, a small but mid-UV bright component of low metallicity ($Z \leq 0.001$) stars may explain the spectral features of NGC 1399. M32's UV features cannot be explained purely by a significant population of intermediate age (1-3 Gyr) solar metallicity stars; a small number of metal-poor stars are suggested by the mid-UV in this case as well. Because metal-poor stars are so much brighter than metal-rich stars in the mid-UV, we cannot ignore the effects of the metallicity distribution on our population synthesis models.

The rest of the paper is arranged as follows: first, in section 2 we test our library of stellar fluxes (Lejeune, Cuisnier, & Buser 1997) for inaccuracies and determine the influence of these inaccuracies on our model spectral energy distributions (SEDs). In section 3, we explain our population synthesis models, their mid-UV and optical properties, and compare them to the mid-UV features of several composite globular cluster IUE spectra (Bonatto, Bica, & Alloin 1995). In section 4, we present the FOS spectra of NGC 1399 and NGC 3610 and the IUE spectra of NGC 1399, M32 and the bulge of M31. We compare our models to these galaxies. In section 5 we examine the effects of a metal-poor sub-population on the integrated spectra of an otherwise metal-rich population.

2. Testing Kurucz Stellar Fluxes

In order to examine the effect of abundance on the integrated light of old stellar populations, Kurucz model stellar fluxes (Lejeune et al. 1997) with $[\text{Fe}/\text{H}] = -1.5, -1.0, -0.5, 0.0,$ and $+0.5$ were used for our population synthesis models. Due to the paucity of non-solar abundance stars in empirical libraries, the Kurucz models offer the advantage of the studying the effects of a full range of metallicity on the model stellar populations. However, at cooler temperatures the model fluxes do suffer from serious limitations. Morossi et al. (1993) compared late G and K solar chemical composition giants and found that, while the optical and infrared observations matched the Kurucz fluxes, significant discrepancies existed in the UV. They concluded that the models failed to account for chromospheric emission and thus under-

estimated the flux at wavelengths less than 3100 Å. Also, the optical Mg₂ index of cool, metal-rich giants may not be well modeled by the Kurucz stellar fluxes. When the Kurucz 1992 models were compared to the improved Kurucz 1993 models, Chavez, Malignini, & Morossi (1995) found that for $T_{\text{eff}} \leq 5000\text{K}$ and $[\text{Fe}/\text{H}] \geq 0.0$, the newer models predicted a Mg₂ values up to 0.58 magnitudes stronger than the 1992 models. The Kurucz 1993 fluxes corrected an error in the FeI continuum opacity for cool stars, had more optical depth points, and included detailed modeling of scattering effects in the source function not accounted for in the 1992 fluxes. Clearly, while the Kurucz models are powerful tools for the modeling of stellar populations, a detailed understanding of their limitations is necessary to interpret the results of our model stellar populations correctly.

Here we quantify the accuracy of the Kurucz model stellar fluxes in the mid-UV and the optical. We test the mid-UV spectra and optical features Mg₂ and H β of the solar abundance Kurucz 1992 models against the composite IUE stellar main sequence spectral energy distributions compiled by Fanelli et al. (1990) and standard stars in the Gunn & Stryker (1983) catalog. The importance of the cool giants on the mid-UV and optical portions of our model SEDs is determined.

2.1. $U - B$ v. $B - V$ for dwarfs and giants

We have used the un-calibrated Kurucz model fluxes presented by Lejeune et al. (1997) as our stellar library. Lejeune et al. (1997) have calculated correction functions for each of the Kurucz models in order to yield synthetic broad-band colors which match the empirical color-temperature relations. However, they note that the dwarf stellar fluxes have a negligible optical color correction for $T_{\text{eff}} \geq 3500\text{K}$, and that the color correction is significant for the giants only for $T_{\text{eff}} \leq 4000\text{K}$. Because we use the non-color corrected fluxes, we first tested the un-calibrated solar metallicity model colors against the colors of the stars in the Gunn-Stryker catalog (Gunn & Stryker 1983). The broad band colors U-B and B-V of the Kurucz fluxes match both the giant and dwarf stars in the Gunn-Stryker catalog to within ± 0.2 magnitudes (Figure 1a & b). The coolest red giant colors are least well fit by the Kurucz fluxes, with a discrepancy of ~ 0.2 magnitudes.

2.2. Mid-UV Spectral Indices

Fanelli et al. (1990, 1992) examined the mid-UV spectral morphology of 218 normal stars observed by IUE and found that the spectral lines in the UV are sensitive to and change significantly with spectral types ranging from O to K. We measured the spectral indices Fe2402, B12538, Fe2609, Mg2800, Mg2852, MgWide, and Fe3000 as defined by Fanelli et al. (1990) (Table 1 and Figure 2) for the Kurucz model fluxes corresponding to solar, main-sequence (MS) stars and compared them to the indices of the IUE stellar spectra measured by Fanelli et al. (1990). Unfortunately, few non-solar metallicity stars were observed, and so our discussion is limited to the comparison of solar abundance stars and the corresponding Kurucz models. It is important to note that the “continuum” band passes for these indices contain very little true continuum. Due to the strong line blanketing in the UV, we are forced to use pseudo-continuum band passes around the absorption features to compute indices and our results will depend on the accuracy of the pseudo-continuum as well as that of the absorption features of the stellar models.

In Figure 3a-g, we plot the B-V color against the mid-UV line indices for both the IUE composite spectra (triangles) and Kurucz fluxes (connected crosses). The B-V colors for the Kurucz models were measured using IRAF task synphot.calcphot. Only the B12538 feature is well matched (to better than 0.05 magnitudes) by the full temperature range of Kurucz main sequence model fluxes (Figure 3b). (When the individual IUE spectra are compared to the Kurucz fluxes, the stellar B12538 values show a great deal of scatter about the Kurucz values (Dorman, O’Connell, & Rood 1997). This may be due to noise in the individual IUE spectra or metallicity and gravity variations. The difference in B12538 between a G0V and G0III star is ~ 0.4 magnitudes; the difference between a G0V and G0IV star is much less, ~ 0.03 magnitudes. We examine the composite IUE spectra of stars identified as luminosity class V because these stars will dominate the mid-UV light.) In general, the Kurucz model fluxes for $B-V \leq 0.1$ ($T_{\text{eff}} \geq 8000\text{K}$) match the observed line strengths of IUE data, but overestimate the line strengths for cooler stars ($B-V \geq 0.2$, $T_{\text{eff}} \leq 7000\text{K}$). In particular, the $T_{\text{eff}} = 6000\text{K}$, $\log g=4.5$ solar Kurucz model is too strong by 0.6 magnitudes

for Fe2404, 0.4 for Fe2609, 0.4 for Mg2800, 0.4 for Mg2852, 0.3 for MgWide, and 0.15 too weak for Fe3000. These discrepancies may be due in part to the inevitably incomplete atomic line lists. They may also be the result of departures from LTE, chromospheric emission filling in the mid-UV absorption lines for cooler dwarfs, and opacity due to tri-atomic molecules, none of which are modeled by the Kurucz stellar fluxes.

2.3. Mid-UV Continuum

The continuum of the mid-UV range is strongly sensitive to the metallicity of the stellar population (Fanelli et al. 1990; Dorman et al. 1995). Age may also influence the mid-UV continuum: the spectrum of an old stellar population at 2500 Å is dominated by flux from main sequence turn-off stars, and thus may be used to constrain this turn-off population more closely than the K and M giant dominated optical region of the spectrum. Again, it is important to realize that the vast number of atomic absorption lines in the UV suppress most of the true continuum and what we observe is a pseudo-continuum.

To examine the dependence of this region’s pseudo-continuum on age and metallicity, we have measured the slope of the pseudo-continuum (Δ magnitude/1000 Å) in the 2600 to 3100 Å range of our model simple populations (section 3). The slope of the pseudo-continuum between 2600 and 3100 (hereafter S_{2850}) was estimated using the IRAF V2.11.1 task onedspec.continuum with high rejection set at 3σ and low rejection set at 1σ in order to exclude the effects of the magnesium features at 2800 and 2852 Å on the spectral shape. Again, to determine possible inaccuracies in the model fluxes, we tested S_{2850} of the Kurucz models against S_{2850} of the IUE observations. In Figure 3h, the S_{2850} for the main sequence IUE spectra and Kurucz models are plotted against $B-V$ for the range of slopes observed in the galaxies. The Kurucz models’ pseudo-continua closely match that of the observations (to better than 0.5 Δ magnitude/ 1000 Å), except for the coolest stars ($(B-V) \leq 1.1$). (Note: the color-corrected Lejeune et al. 1997 version of the stellar models do not reproduce S_{2850} ; the shifts in B-V are small but the S_{2850} feature is shallower by up to 2 mag/1000 Å.)

2.4. Mg₂ and H β

We also examine the robustness of the Kurucz models’ line strengths at optical wavelengths for solar metallicity giants. The Mg₂ feature is primarily a measurement of the galaxy’s metallicity, but is also strongly linked to age. The H β feature at 4860 Å is sensitive to main sequence turn-off temperature, and hence may be an indicator of age (Bressan et al. 1996; Gonzalez 1993). Observed elliptical galaxy H β and H γ absorption strengths suggest intermediate ages (≤ 8 Gyr). We seek to determine the relationship between the mid-UV properties and these optical line strengths for elliptical galaxies (section 4).

In Figure 4a-d, we compared the Mg₂ and H β features of the Kurucz solar MS dwarfs and giants models to a number of standard MS dwarfs and giants taken from the Gunn-Stryker atlas. The Kurucz models have an H β equivalent width ~ 1 - 2 Å less than the standard stars, so we do not use this optical feature for our analysis. Although Mg₂ is well modeled by the Kurucz models with $T_{\text{eff}} \geq 4500$ K, cooler giants increasingly overestimate the feature by 0.2 magnitudes or more (Figure 4a). The coolest dwarf models also overestimate Mg₂ strength. Given that Chavez et al. (1995) found that the cool metal-rich giant Kurucz models’ Mg₂ values were strongly sensitive to small changes in the scattering parameter, we will also not use the Mg₂ values estimated by the Kurucz models. Instead we use the empirical fitting formula given by Borges et al. (1995) (the dashed line in Figure 4a,b). Borges et al. (1995) determined the dependence of \sim eighty stars’ Mg₂ on effective temperature, gravity, [Fe/H], and [Mg/H].

2.5. Importance of cool giants on model SEDs

Our model SEDs were created using the technique of “isochrone synthesis”, whereby a stellar population is created by summing up stellar fluxes along isochrones for a given age and metallicity; in section 3 we describe this process in greater detail. Comparing the isochrones of different ages and metallicity (Bertelli et al. 1994), we see that old, metal-rich populations possess a significant number of K and M giants. Since the Kurucz stellar fluxes poorly model these stars in the UV, we examined the importance of the cool giants to the

total integrated light of our oldest, most metal-rich (20 Gyr, $Z=0.05$) model population.

We have removed the contribution from giant stars with $T_{\text{eff}} \leq 4500$ K from a 20 Gyr, $Z=0.05$ SED and compared it to the un-modified SED (Figure 5). We see that the giants contribute very little light to the mid-UV (1800-3200 Å), and become significant for wavelengths ≥ 4000 Å. Thus we are confident that the mid-UV continuum of our synthetic populations is not significantly affected by the known inaccuracies of cool giants.

In summary, after close investigation of the mid-UV and optical line strengths of the main sequence and giant solar metallicity Kurucz models, we are left with only the blend feature of FeI and MgI at 2538 Å in the mid-UV ($B/2538$) and the slope of the continua between 2600 and 3100 Å ($S2850$) as features reproduced well by the Kurucz models. We are satisfied that the mid-UV is not significantly influenced by the discrepancies in the cool giant stellar models. However, if further detailed investigation of the narrow band absorption features in the mid-UV is to be done, new model stellar fluxes with more accurate mid-UV and optical line strengths need to be constructed. It is important to note that our tests of the $B/2538$ and $S2850$ features have only shown that the relative fluxes of the pseudo-continuum over small wavelength regions are reasonably matched by the Kurucz models. For $B/2538$, we have only examined the relative flux of the local pseudo-continuum to the blend absorption feature, and for $S2850$, we have tested the average slope of the pseudo-continuum over a 500 Å range. A 10 % error in the mid-UV pseudo-continuum would introduce a 0.1 magnitude error in $B/2538$ and a 0.2 magnitude/ 1000 Å error in $S2850$. Problems with the mid-UV pseudo-continuum over larger wavelength regions and its normalization relative to the optical pseudo-continuum may still exist.

3. Single metallicity stellar population models

3.1. Spectral synthesis

Single metallicity, single age simple stellar populations were constructed using the “isochrone synthesis” technique, which sums up model stellar fluxes using a given set of isochrones, IMF and star formation rate. We used Kurucz model fluxes

for stars with $3500 \text{ K} \leq T_{\text{eff}} \leq 40000 \text{ K}$, the Padova isochrones (Bertelli et al. 1994), a Salpeter IMF, and an exponentially decaying star formation rate with $\tau = 10^7$. Spectral energy distributions were created for $Z=0.0004, 0.001, 0.008, 0.02,$ and 0.05 and ages 3, 7, 10, 12, 15, and 20 Gyrs. Further details of the isochrone synthesis code are given in Babul & Ferguson (1996).

The Padova isochrones only contain “normal” P-AGB stars and do not model post-early AGB (PE-AGB), AGB-manqué or “extreme blue horizontal branch” stars (HB stars with ZAHB $T_{\text{eff}} \geq 16,000$ K) which are all possible contributors to the UV upturn found in elliptical galaxies (Brown et al. 1997). While the existence of EHB stars and their descendents in elliptical galaxies is reasonably secure observationally, theoretical models of how the EHB is populated are uncertain. The number of EHB stars depends on parameters such as the metallicity, age, helium abundance of the stellar population, and on the details of mass loss at the tip of the red giant branch. While it is possible to choose plausible values for these parameters and construct synthetic spectra, the dependence on the poorly constrained RGB mass loss rate means that the UV upturn is not yet useful for constraining the age and chemical content of the stellar population.

For galaxies with a strong UV upturn, the mid-UV portion of the spectrum contains flux both from EHB stars ($T_{\text{eff}} \sim 25,000$ K) and from cooler HB and MS turn-off stars. Because we are interested in the MS turn-off stars, we have chosen to subtract the hot stellar component from both the models and the data (section 4). The isochrones were modified to eliminate HB and P-AGB stars with $T_{\text{eff}} \geq 9,000$ K (Figure 6). With these modified tracks, spectral energy distributions were created for $Z=0.0004, 0.001, 0.008, 0.02,$ and 0.05 and ages 3, 7, 10, 15, and 20 Gyrs.

3.2. Mid-UV and Mg_2

In section 2, we evaluated the accuracy of the Kurucz models and found that the blend feature at 2538 Å and the slope $S2850$ were well modeled. We measured $B/2538$ and $S2850$ for the single age (3 - 20 Gyr), single metallicity ($Z=0.0004 - 0.05$) models. Mg_2 was calculated using the empirical

formula from Borges et al. (1995):

$$Mg_2 = \exp\{-9.037 + 5.795 \cdot \theta + 0.398 \cdot \log g + 0.389 \cdot [Fe/H] - 0.16 \cdot [Fe/H]^2 + 0.981 \cdot [Mg/Fe]\}, \quad (1)$$

where $\theta = 5040/T_{\text{eff}}$ (plotted as a dashed line in Figure 4a,b). Because the Kurucz model stellar fluxes do not model the effect of enhanced α element abundance on the mid-UV spectrum, we assumed $[Mg/Fe] = 0$. An enhanced $[Mg/Fe]$ has a strong effect on Mg_2 at the higher metallicities; a 15 Gyr, $[Fe/H]=0.0$, $[Mg/Fe]=+0.5$ population has a Mg_2 feature 0.15 magnitudes stronger than a similar $[Mg/Fe]=0.0$ population.

In Figures 7-9 we plot the relations between $Bl2538$, $S2850$, and Mg_2 as a function of age and metallicity. The models generally occupy a narrow locus on these figures, indicating an age-metallicity degeneracy for simple stellar populations. However, young metal-rich populations do not overlap with old metal-poor populations due to the curvature in the relations shown in Figures 7 and 9. This curvature also means that populations with a spread in metallicity will not follow the simple stellar population locus. We will return to this in section 5.

3.3. Testing Models against Globular Clusters

The tests of the Kurucz model fluxes in section 2 were valid only for solar metallicity. In this section we compare the features predicted by the simple stellar population models to the observed features in globular clusters to test the synthesis model’s validity at low metallicity and old ages. Bonatto et al. (1995) published mid-UV equivalent widths (EW) and continuum point relative flux values normalized to the flux at 2646 Å for composite globular cluster IUE spectra (Table 2). We chose the seven composite spectra for globular clusters with ages ≥ 10 Gyr and metallicities $Z=0.0002$ to 0.006 to test the validity of the slopes and mid-UV $Bl2538$ features of our simple models. We are not able to estimate the hot stellar component of the integrated globular cluster spectra because the full spectra are not given. Therefore we computed our model SEDs with the original isochrones (including the hot HB and post HB stars) and compared these to the composite glob-

ular cluster features (Figure 10). The presence of the hot stellar component has little effect on the low metallicity models, but significantly changes the $Bl2538$ feature for the $Z \geq 0.02$ models.

Bonatto et al. (1995) measure the equivalent width between 2506-2574. This is approximately 40 Å wider than the $Bl2538$ index, and encompasses SiI absorption lines at 2507, 2514, 2516, thus translating this EW into an index may cause a slight overestimation of the strength of the $Bl2538$ index. Fitting the slope of the globular cluster spectra was relatively straight-forward. The slope of a line fit to the log of the flux at the continuum points 2646, 2959, and 3122 Å was measured. In order to convert the equivalent widths to indices, the flux of the continuum for the EW bandpass at 2556 Å (C_{2556}) was interpolated between the continuum flux at 2466 Å and 2646 Å. Then the “area” of the absorption feature was determined by multiplying the EW by this interpolated continuum flux C_{2556} . Then the depth of the absorption feature was estimated by dividing this area by the width of the EW bandpass (68 Å). Finally the flux of the absorption feature at 2556 Å (F_{2556}) was calculated by subtracting the depth of the absorption feature from C_{2556} and the $Bl2538$ index value was estimated by $-2.5 \log(F_{2556}/C_{2556})$.

Table 2 gives the EW and continuum values measured by Bonatto et al. (1995), and the calculated indices and slopes. The calculated indices and slopes have large uncertainties, since these values are only rough estimates from the data. Nevertheless, plotting the globular cluster points (triangles) on Figure 10, we find good agreement with our simple SEDs, except for 47 Tuc. The difference between the globular clusters (except for 47 Tuc) and the models is ≤ 0.05 in $Bl2538$ and ≤ 0.35 in $S2850$. When the EW of our $Z=0.0004$, 0.001 , and 0.008 , 15 Gyr model SEDs were measured, they agree well with the globular cluster EW although the model $Z=0.008$ EW is slightly less than the clusters’ EWs. The globular clusters’ slopes and $Bl2538$ strengths increase with metallicity, as predicted by our single age, single Z models.

Note that the cluster slopes are slightly lower than the model predictions (although within the uncertainties), which may be due an underestimation of the slope of the clusters because of uncertainties in the hot HB and post HB stellar

component. The Padova isochrones do not possess extreme horizontal branches, which may affect the mid-UV light of some of the globular clusters. Note the difference between the the “blue” $Z=0.0007$ cluster and the “red” $Z=0.0006$ cluster in B12538. Again, this may be the result of the blue component of stars washing out the B12538 feature.

3.4. Reddening effects

The effects of interstellar extinction on the S2850 and B12538 were found to be less than the uncertainty of the model SEDs and galaxy data. Galactic extinction curves with $A_B = 0.0, 0.05, 0.10, 0.25, 0.50,$ and 0.75 (Pei 1992) were used to redden the SEDs of solar metallicity models of ages 1, 3, 7, 10, 15, and 20 Gyr and the SEDs of a 7 Gyr population with $Z= 0.0004, 0.001, 0.008, 0.02,$ and 0.05 . In all cases, $\Delta B12538 \leq 0.05$ magnitudes. For $A_B \leq 0.50$, $\Delta S2850 \leq 0.4$ and was 0.6 for $A_B = 0.75$. Thus, for Galactic reddening with $A_B \leq 0.50$, the reddening effects on the slope and the blend feature are less than the error bars on the galaxy data points (Figure 7).

4. Galaxy spectra

4.1. FOS observations of NGC 1399 and NGC 3610

NGC 1399 and NGC 3610 were observed with the HST Faint Object Spectrograph on 1993 17 January and 1992 30 November, respectively (Figure 11). Gratings and exposure times are shown in Table 3. All observations used a $1.0''$ diameter circular aperture. The observations were with the aberrated HST optics, prior to installation of COSTAR. In this paper we focus on the G270H data.

The target acquisition procedure involved measuring the flux a 4×4 grid for spaced at $0.25''$ intervals, and choosing the brightest spot in the grid. This procedure thus centered the galaxy to an accuracy of $0.25''$ in the aperture, and also resulted in the observations with the red channel and the blue channel being slightly offset from each other (in retrospect a 5×5 grid would have been better).

The FOS data were reduced following standard pipeline procedures. This involves correcting for geomagnetic-induced image motion; correcting for

particle-induced dark current based on the geomagnetic position of the spacecraft; correcting for scattered light via subtraction of a constant count-rate determined from diodes that are unilluminated by the selected grating; flat-field correction; wavelength calibration; and flux calibration based on observations spectrophotometric standards.

A full correction for grating-scattered light is in principle much more complex than the simple subtraction of a constant we have adopted here (Bushouse, Rosa, & Mueller 1995). In particular, due to the high sensitivity of the FOS detectors to long-wavelength photons, the FOS spectra contain a component of light scattered from wavelengths longward of 3000 \AA . We have used bspec (Rosa 1994) to estimate the uncertainty introduced by ignoring the wavelength dependence of the scattered light correction. For NGC1399 we use a composite spectrum constructed from the the HUT spectrum, the IUE spectrum of NGC4649, and an optical spectrum from the Las Campanas Observatory (Kimble, Davidsen, & Sandage 1989), normalized to agree in the wavelength regions where they overlap. For this model, the average scattered light contribution to the measured flux from $1700\text{-}3270 \text{ \AA}$ is less than 1%.

4.2. IUE observations

We have obtained UV spectra for NGC 1399, M32 and the bulge of M31, extracted from the IUE database by D. Calzetti (Figure 11). All the spectra have been corrected for redshift obtained from NED using the IRAF V 2.11.1 task oned-spec.dopcor. Literature values for Mg_2 (Burstein et al. 1988; Worthey, Faber, & Gonzalez 1992) may overestimate the galaxy’s mean Mg_2 index strength because the spectra are often taken with a narrow aperture centered on the inner-most (and probably most metal-rich) regions of the galaxy. We measure the Mg_2 values from the optical spectra of Kinney et al. (1996) which were taken with an aperture matched to the $10'' \times 20''$ IUE aperture. For NGC 1399, $20''$ corresponds to ~ 2 kpc. However, for M 31 and M 32, $20''$ corresponds to ~ 80 pc, so for these galaxies even with the wide aperture slit we are observing only the very central regions.

In the case of NGC 3610, wide aperture optical spectra were not available and the Mg_2 value taken with the Lick $1.4'' \times 4''$ aperture (Worthey

et al. 1992) was compared to our models. If we assume NGC 3610 has a metallicity gradient typical of other elliptical galaxies (Davies et al. 1993; Carollo et al. 1993), no appreciable age gradient, and an age ~ 10 Gyr, at a $10''$ radius, NGC 3610 should have a slope 0.5 magnitudes/1000 Å less steep, B12538 0.05 magnitudes weaker, and an Mg_2 0.05 magnitudes weaker than measured in a $1''$ aperture.

4.3. Hot component subtraction

Our goal is to examine the main sequence and cooler stellar sub-population of these galaxies, and not the hot horizontal and post HB populations. We must therefore determine which galaxies possess significant UV upturns and attempt to subtract away this hot component of the spectra. We estimated the strength of the UV upturn by measuring the 1550 – 2500 color of the galaxies with the IRAF task onedspec.sband. The 1550 and 2500 bands were centered at 1550 and 2500 Å respectively and were both 600 Å wide. Our calculations of 1550 – 2500 agreed with previously published values for the galaxies.

M32 had the reddest 1550 – 2500 color (~ 1.5). The rest of the galaxies have significant UV upturns indicative of a hot stellar population. Ferguson & Davidsen (1993) found that the far-UV flux of M31 shows a drop-off blue-ward at 1000 Å, which requires that the T_{eff} be $\sim 25,000$ K for the UV emitting stars. Thus, for the “normal” galaxies with no recent star formation, the UV upturn can be roughly approximated by a $T_{\text{eff}} \sim 20000$ - 30000 K star. Between 1350 and 3200 Å, the spectral shape changes very little with temperature for stars hotter than 20,000 K. For the galaxies with 1550-2500 colors ≤ 0.5 magnitudes, we fit a 20,000K $\log g=5$ Kurucz model to the galaxies’ flux between 1350 and 1650 Å and subtracted the stellar spectrum from the galaxies spectra (Figure 12). To test whether this method did a good job of eliminating the light from the hot component, models of a simple single metallicity population were created using the original isochrones with hot HB and P-AGB stars. Then the 20,000 K stellar model was fit and subtracted from this model SED. The resulting spectra had an identical slope and B12538 strength as the model created using the modified isochrones (section 3.1). Thus if a galaxy’s UV upturn is due to a $\sim 20,000$ K hot

stellar component, the subtracted galaxy spectra should have S2850 and B12538 which reflect the metallicity and ages of the cooler stars.

If a significant population of “blue stragglers” with $T_{\text{eff}} \sim 10,000\text{K}$ exists, the resulting spectra will still have contamination from this non-MSTO population. However, like the hot HB and post HB population, the blue straggler population in galaxies is not well constrained. Spinrad et al. (1997) estimate that if elliptical galaxies have blue straggler populations similar to that of old metal-poor clusters, blue stragglers may contribute as much as 20-50 % of flux at 2600 Å. On the other hand, for the higher metallicity cluster 47 Tuc, the blue straggler contribution to the mid-UV flux has been estimated to be 7% (Rose & Deng 1999).

4.4. General trends in spectral features

Figures 7-9 show the measured spectral indices for the four galaxies in our sample. While the sample is small and the error bars are large, there are at least hints of some general trends. In particular, as Mg_2 increases, the B12538 feature tends to get weaker and the slope S2850 tends to get shallower. This is clearly evident in the comparison of NGC 1399 ($Mg_2 = 0.312$) and NGC 3610 ($Mg_2 = 0.271$) in Figure 11. It is also clear in Figure 7-9 that the galaxies do not follow the behavior expected for simple stellar populations. The galaxies are generally displaced from the model locus and the trends are nearly orthogonal to those expected for simple variations of age and metallicity.

5. Bi-modal metallicity models

Our understanding of chemical evolution dictates that galaxies, unlike star clusters, have complex chemical make-ups, and so the comparison of single metallicity SEDs to real galaxies is limited in its usefulness. Color and Mg_2 line strength gradients with galactic radius (Davies et al. 1993) and the width of the RGB in M32 (Grillmair et al. 1996) are evidence of stellar populations of varying metallicities within ellipticals. However, the details of the metallicity distribution in ellipticals are not well understood. Comparing the Mg_2 and Fe line strengths for synthetic populations and observed galaxies, Greggio (1997) finds high average metallicities, small metallicity dispersions and old ages for ellipticals. Worthey et al. (1996) find

that for M31 and M32 and Bressan et al. (1994) find that for NGC1404 and NGC4649 only $\leq 10\%$ by mass of stars are metal poor ($Z \leq 0.008$), which suggests that the ‘G dwarf problem’ is not limited to the disk of the Galaxy.

Because simple, single abundance SEDs did not match the mid-UV features of the majority of the galaxies in our sample, we looked to see how a spread in metallicities affects the light of a single stellar population. We consider a very simple bi-modal metallicity scenario for old stellar populations. Two different bi-modal metallicity models are created by combining the spectra of the metal-poor $Z=0.0004$ 12 Gyr population with the metal-rich spectra $Z=0.05$ or $Z=0.02$ 12 Gyr populations. The models are constructed so that 0.5%, 1%, 5%, 10%, and 15% of the total galaxy mass originates from the metal-poor $Z=0.0004$ sub-population. These bi-modal metallicity models are then measured for B12538, Mg_2 , and $S2850$. Figure 13 shows the combined 10% $Z=0.0004$ mass and 90% $Z=0.05$ mass 12 Gyr model (solid line) and each of its sub-population SEDs (short dashed line for $Z=0.0004$, long dashed line for $Z=0.05$). While the metal-rich component dominates the visible light, the metal-poor component dominates the mid-UV. (Table 5)

In Figures 14a,b,c we show the single metallicity models for a given age and the results of the bi-modal metallicity populations. The $Z=0.05 / Z=0.0004$ models are represented by the pentagons where the model with the highest slope and smallest pentagon has 0.5% of its mass from the metal-poor sub-population and the model with the lowest slope and largest pentagon has 15 % of its mass from the metal-poor sub-population. The $Z=0.02 / Z=0.0004$ models are represented by stars, again with the smallest star representing the 0.5% metal-poor mass model and the largest star representing the 15% metal-poor mass model.

Comparing the bi-modal models with the galaxies, we see that the positions of most of the galaxies in the $S2850$ v. B12538 plane may be explained by a significant contribution of a metal-poor stellar population to the flux at 2600 Å (Figure 14a). On the other hand, contamination by “blue stragglers” or problems with the hot component subtraction may also result in weaker mid-UV features. But it is important to note that a small percentage of metal-poor stars can contribute most of

the light at 2600 Å. While our results do not predict the number of low metallicity stars needed to “solve” the G-dwarf problem, it is not unreasonable to expect a few low metallicity stars in ellipticals. However, except for NGC 1399, for which the bi-modal metallicity tracks fit particularly well in all three planes, the Mg_2 strengths are slightly too strong to agree with most of the galaxies.

6. Discussion

The combination of B12538, $S2850$, and Mg_2 provides a unique tool for investigating elliptical galaxy evolution. The UV features are most responsive to changes in the effective temperature of the turn-off population, while Mg_2 to first order measures the effective temperature of the giant branch. The positions of the galaxies in the line-strength vs. line-strength diagrams suggest: (a) these galaxies are not well represented by simple (single-age, single-metallicity) populations, and (b) that the star-formation and chemical enrichment histories were unique and complex. The addition of a small metal-poor component to a dominant old, metal-rich component helps to reconcile the models to the data.

Part of the difficulty in understanding the observations probably stems from the heterogeneous nature of the sample of galaxies in our sample, which to a certain extent represent the extremes of phenomena seen in elliptical galaxies, rather than the norm. It is thus worth considering each galaxy in turn, and examining the UV results in the context of other information about the galaxy.

M32: M 32, a compact E1 satellite of M 31, is the closest example of an elliptical galaxy. M 32 is unusual in that it has a very weak Mg_2 feature and no UV upturn. The stellar population in this galaxy has been the subject of intense study, both via integrated light and via the resolved stellar population. Based on its blue (B-V) color, and on spectral synthesis, O’Connell (1980) has suggested that it contains a ~ 5 Gyr subpopulation. The population synthesis study of Bressan et al. (1994) found that M 32 spectrum is dominated by a 13-15 Gyr, $Z \leq Z_\odot$ population, and has evidence for an additional 5 Gyr stellar population. The mid-UV region of M 32’s spectrum is not well fit by the closed box enrichment model and is more closely matched when the contribution from $Z \leq$

0.008 stars is removed. In Bressan et al. (1994) and later in Tantalo et al. (1996), the infall of gas is suggested as a mechanism for increasing the galaxy’s metallicity quickly and preventing the formation of a significant number of metal-poor stars. HST photometry a few arcminutes from the M 32’s nucleus (Grillmair et al. 1996) seems to have confirmed the dominance of old solar metallicity stars and the deficiency of metal-poor stars. The observed width of the red giant branch requires that at least half of the stars in M 32 be older than 8 Gyr. Grillmair et al.’s study also requires that the stars span a wide metallicity range but are strongly skewed to solar abundances.

Based on the comparison of IUE mid-UV observations of M 32’s nucleus with the globular cluster 47 Tuc, Rose & Deng (1999) found the mid-UV spectrum of M 32 was best fit by a combination of a solar metallicity MSTO, a solar giant branch, and a hot A star component consisting of metal-poor stars and possibly some P-AGB stars. The mid-UV spectral breaks 2609/2660 and 2828/2923 and absorption features Mg2800 and Mg2852 are weaker in M 32 than in 47 Tuc, but the C26-30 color (similar to our *S*2850) is redder in M 32. While Rose & Deng (1999) were able to reproduce the spectral breaks and absorption lines with a solar MSTO population with a $\sim 25\%$ metal-poor contribution of the mid-UV light, the simulated C26-30 color was ~ 0.1 magnitude bluer than M 32. Since this color is dominated by the MSTO whereas the other features are influenced more by the hotter population, a slightly higher metallicity MSTO may reconcile the simulation with M 32.

From the simple single age, single metallicity SEDs (Figures 7-9), we see the mid-UV and Mg₂ are not consistent with a single metallicity. The slope of M32 points to a dominant population with a metallicity $Z \geq 0.02$, the mid-UV B12538 value implies a lower metallicity population of $Z \sim 0.001-0.008$, and Mg₂ gives a $Z \sim 0.008 - 0.02$ population. Invoking a bi-modal abundance model improves the situation slightly. The 12 Gyr, 0.5% $Z=0.0004$ / 99.5% $Z=0.05$ SED matches the UV features, but gives a Mg₂ value stronger than what is observed (Figure 14a-c). We have also modeled the mid-UV features for composite $Z=0.05$ populations with both a 12 Gyr and 3 Gyr population (Figure 15). While the *S*2850 of M 32 is matched by 5% 3 Gyr / 95% 12 Gyr $Z=0.05$ composite

population, the B12538 of the composite model is too strong. Solar metallicity composite 3 Gyr/12 Gyr populations would also have B12538 features stronger than M 32 and shallower slopes. Figure 16 shows a direct comparison between the M 32 spectra, the best fitting metal-poor component model (0.5% $Z=0.0004$ / 99.5% $Z=0.05$ 12 Gyr), and the best fitting young component model (5% 3 Gyr / 95% 12 Gyr $Z=0.05$). The slopes are identical for M 32 and the two models, but the B12538 of the multi-metallicity model agrees more closely with M 32. A more complex model with a distribution of metallicities and ages may reproduce both Mg₂ and the mid-UV.

Invoking an intermediate 3-5 Gyr metal-rich sub-population is not sufficient to explain M 32’s UV features; the presence of a small number of metal-poor stars is implied. The number of low abundance stars predicted is very small ($\sim 0.5\%$). This agrees with Bressan et al. (1994) and Grillmair et al. (1996) result of a deficiency of M 32 metal-poor stars as compared to a closed box chemical evolution model. However, the existence of a 2-5 Gyr metal-rich population is not ruled out. The steep slope of M 32’s spectrum seems to require a $Z > Z_{\odot}$ MSTO population (Figures 14a, 15). It is important to note that our mid-UV M 32 spectrum is of only the inner-most 80 pc, hence we may be observing the most metal-rich region of the galaxy, whereas the HST color magnitude diagram (Grillmair et al. 1996) which gives a peak abundance $\sim Z_{\odot}$ is of a region ~ 500 pc from the nucleus.

Bulge of M31: M 31 has one of the reddest and strongest absorption-featured bulges known. Its Mg₂ index in the innermost regions is comparable to that found for ellipticals and α element enhancement has been suggested (Davidge 1997). However, its H β strength (Davidge 1997) and the reported presence of luminous AGB stars suggest an age younger than our Galactic halo of $\sim 8-10$ Gyr (Rich & Mighell 1995). Absorption line gradients suggest that the mean stellar population becomes older and more metal poor with increasing radius (Davidge 1997).

Like M 32, the spectral features can not be fit by a single metallicity model and are more consistent with an additional low abundance population. In Figures 7-9, we find that both Mg₂ and *S*2850 are consistent with high metallicity ($Z \geq$

0.02) dominant population, while B12538 gives a lower metallicity ($Z \sim 0.001$). The 12 Gyr, 0.5 % $Z=0.0004$ / 99.5 % $Z=0.05$ model matches M 31 in the mid-UV, but produces a slightly stronger Mg_2 than observed (Figure 14 a-c). The mid-UV features of the bulge of M 31 suggest a small number of metal-poor stars ($\leq 1\%$ by mass), while its Mg_2 may point to the contribution of a metal-rich, intermediate age population.

NGC 3610: This galaxy has many properties of a 3 - 7 Gyr merger remnant: NGC 3610 has the richest fine structure measured for an elliptical; it has an unusually blue color; and it possesses a weak Mg_2 feature and an enhanced $H\beta$ absorption (Schweizer et al. 1990; Schweizer & Seitzer 1992). There is not a significant amount of dust or cold gas in the galaxy, nor is there any evidence for ongoing star formation. HST observations have detected a number of red globular clusters in NGC 3610, consistent with an age of 4 Gyr (Whitmore et al. 1997).

Comparison with the single age, single metallicity SEDs shows that NGC 3610's slope and Mg_2 are consistent with high metallicity ($Z \geq 0.02$) dominant population, while the B12538 feature implies a lower metallicity ($Z \sim 0.001$). The 12 Gyr, 1% $Z=0.0004$ / 99% $Z=0.05$ model is consistent with the mid-UV features, but predicts a slightly stronger Mg_2 value than observed in NGC 3610. Here again, we detect the signature of a small number of metal-poor stars ($\leq 1\%$ by mass) in the mid-UV light, and while the Mg_2 feature may be influenced by a population of metal-rich 3 - 7 Gyr stars.

NGC 1399: This gE in has one of the strongest Mg_2 values and UV upturns known. Like other gEs, NGC 1399 is thought to be old and very metal-rich. NGC 1399 possesses ~ 5800 globular clusters; recent Keck spectroscopy (Kissler-Patig et al. 1998) of ~ 20 of these clusters give a mean $[Fe/H] \sim -0.8$ dex and found no very metal-poor clusters (although the sample may have been biased against blue clusters).

Surprisingly, both mid-UV features point to a low metallicity population when compared to the simple models, while the Mg_2 implies a high metallicity dominant population. The 12 Gyr model with 5-10% $Z=0.0004$ / $Z=0.05$ agrees with the mid-UV features and Mg_2 of the IUE data. The FOS data, which observes only the center-most

region of NGC 1399, imply an even higher metallicity and/or a lower metallicity population. Using the Borges et al. (1995) calibration (equation 1), a $Z \sim 2 \times Z_{\odot}$, $[Mg/Fe] = 0.0$, 10-15 Gyr model is sufficient to explain the mean NGC 1399 Mg_2 value obtained by the wide $10'' \times 20''$ aperture (Section 4.2, Table 4). An α enhanced ($[Mg/Fe] > 0.0$) model is not required to explain NGC 1399's strong Mg_2 , but not ruled out. *NGC 1399 appears to have the greatest percentage of low abundance stars ($\sim 10\%$), indicating a broader metallicity distribution than less massive ellipticals.* The strength of Mg_2 may rule out the existence of an intermediate age population.

7. Conclusions

We have attempted to set additional constraints on the evolution of elliptical galaxies and spiral bulges by analyzing their mid-UV spectra. Through comparisons IUE observations of individual stars to the Kurucz-model fluxes, two spectral indices (B12538 and S2850) are identified that appear to be promising diagnostics of the main-sequence turn-off population (given the current generation of model stellar fluxes).

Single metallicity, single age model populations are constructed and found to agree well with the mid-UV features of globular clusters. However most of the of the galaxies do not fall on the single-age, single-metallicity tracks. Contamination by blue stragglers may be partially responsible. Another explanation is that the flux from metal-poor stars, invisible in the optical region of the spectrum, begins to dominate the flux in the mid-UV. In order to determine the effect of a small percentage (by mass) of metal-poor stars on the SED of an otherwise metal-rich population, simple single age, bi-modal metallicity models were created. For all the galaxies, a small ($\leq 10\%$ by mass) number of low metallicity stars are implied by the mid-UV features. Metal-poor stars are of course expected from chemical-evolution arguments, but evidence for a metallicity spread has been hard to find in the optical spectra. The metallicity distribution function can no longer be ignored if we hope match simultaneously the mid-UV and the optical spectra.

It is difficult to draw strong conclusions about the recent star-formation history of the galaxies in

our sample from the mid-UV. NGC 1399, one of the strongest Mg₂ and UV upturn galaxies known, is consistent with a multi metallicity 12 Gyr model in both the mid-UV and Mg₂ strength and may possess the greatest percentage of low metallicity stars observed. The strength of Mg₂ suggests that NGC 1399 has few, if any, stars younger than 10 Gyr. However, for the remaining galaxies, especially M 32, a more sophisticated model invoking both old metal-poor and intermediate age metal-rich stars may be needed to reconcile the Mg₂ and mid-UV features. On the other hand, variations the blue straggler populations and α element abundance could also account for the disparities between the optical and mid-UV spectra.

Because they probe the main-sequence turn-off population, mid-UV spectral diagnostics can in principle provide a a powerful diagnostic of the star-formation history and chemical evolution of elliptical galaxies. Our study presents a rather discouraging, but nevertheless realistic, picture of the current status of the models and the data in this wavelength regime. The mid-UV features we have identified suggest that significant progress can be made with additional high-quality spectra of elliptical galaxies, even if the model stellar fluxes do not improve. However, the promise of this wavelength regime for untangling long-standing issues of galaxy evolution should also motivate attempts to improve the model stellar fluxes, which will ultimately put such analyses on firmer ground, and allow the use of additional spectral features.

We wish to thank the referee for his many constructive comments and suggestions. We also thank Daniela Calzetti and Anne Kinney for allowing us to use their extracted IUE and optical spectra, and Michael Gregg for useful discussions about M 32. This paper is based in part on observations with the NASA/ESA Hubble Space Telescope obtained at the Space Telescope Science Institute. Support for this work was provided by NASA through grant number GO-03647.01-91A from the Space Telescope Science Institute, which is operated by the Association of Universities for Research in Astronomy, Incorporated, under NASA contract NAS5-26555.

REFERENCES

Babul, A. & Ferguson, H. C. 1996, *ApJ*, 458, 100

- Bertelli, G., Bressan, A., Chiosi, C., Fagotto, F., & Nasi, E. 1994, *A&AS*, 106, 275
- Bonatto, C., Bica, A., & Alloin, D. 1995, *A&AS*, 112, 71
- Borges, A. C., Idiart, T. P., de Freitas Pacheco, J. A., & Thevenin, F. 1995, *AJ*, 110, 2408
- Bressan, A., Chiosi, C., & Fagotto, F. 1994, *ApJS*, 94, 63
- Bressan, A., Chiosi, C., & Tantalo, R. 1996, *A&A*, 311, 425
- Brown, T. M., Ferguson, H. C., Davidsen, A. F., & Dorman, B. 1997, *ApJ*, 482, 685
- Burstein, D., Bertola, F., Buson, L. M., Faber, S. M., & Lauer, T. R. 1988, *ApJ*, 328, 440
- Bushouse, H., Rosa, M., & Mueller, T. 1995, in *Astronomical Data Analysis Software and Systems IV*, ed. R. A. Shaw, H.E. Payne, & J. J. E. Hayes (ASP Conference Series), 345
- Carollo, C. M., Danziger, J. J., & Buson, L. 1993, *MNRAS*, 265, 553
- Charlot, S., & Bruzual, G. A. 1991, *ApJ*, 367,126
- Charlot, S., Worthey, G., & Bressan, A. 1996, *ApJ*, 457, 625
- Chavez, M., Malagnini, M. L., & Morossi, C. 1995, *ApJ*, 440, 210
- Davidge, T. J. 1997, *AJ*, 113, 985
- Davies, R. L., Sadler, E. M., & Peletier, R. F. 1993, *MNRAS*, 262, 650
- Dorman, B., O'Connell, R. W., & Rood, R. T. 1995, *ApJ*, 442, 105
- Dorman, B., O'Connell, R. W., & Rood, R. T. 1997, *BAAS*, 191, 4903
- Faber, S. M., Friel, E. D., Burstein, D., & Gaskell, C. M. 1985, *ApJS*, 57, 711
- Fanelli, M. N., O'Connell, R. W., Burstein, D., & Wu, C. C. 1990, *ApJ*, 364, 272
- Fanelli, M. N., O'Connell, R. W., Burstein, D., & Wu, C. C. 1992, *ApJS*, 82, 197

- Ferguson, H. C., & Davidsen, A. F. 1993, ApJ, 408, 92
- Gonzalez, J. J. 1993, PhD. thesis, UC Santa Cruz
- Greggio, L. 1997, MNRAS, 285, 151
- Grillmair, C. J. et al. 1996, AJ, 112, 1975
- Gunn, J. E., & Stryker, L. L. 1983, ApJS, 52, 121
- Heap, S. R., et al. 1998, ApJ, 492, 131
- Kimble, R. A., Davidsen, A. F., & Sandage, A. 1989, ApJS, 157, 237
- Kinney, A., Calzetti, D., Bohlin, R. C., McQuade, K., Storchi-Bergmann, T., & Schmitt, H. R. 1996, ApJ, 467, 38
- Kissler-Patig, M., Brodie, J. P., Schroder, L. L., Forbes, D. A., Grillmair, C. J., & Huchra, J. P. 1998, AJ, 115, 105
- Lejeune, T., Cuisnier, F., & Buser, R. 1997, A&AS, 125, 229
- Morossi, C., Franchini, M., Malagnini, M. L., Kurucz, R. L., & Buser, R. 1993, *â*, 277, 173
- O'Connell, R. W. 1980, ApJ, 236, 430
- Park, J. H., & Lee, Y. W. 1997, ApJ, 476, 28
- Pei, Y. C. 1992, ApJ, 395, 130
- Rich, R. M. & Mighell, K. J. 1995, ApJ, 439, 145
- Rosa, M. 1994, FOS ISR 127
- Rose, J. A. 1994, AJ, 107, 206
- Rose, J. A., & Deng, S. 1999, AJ, 117, 2213
- Schweizer, F. & Seitzer, P. 1992, AJ, 104, 1039
- Schweizer, F., Seitzer, P., Faber, S. M., Burstein, D., Ore, C. M. D., & Gonzalez, J. J. 1990, ApJ, 364, 33
- Spinrad, H., Dey, A., Stern, D., Dunlop, J., Peacock, J., Jimenez, R., & Windhorst, R. 1997, ApJ, 484, 581
- Tantalo, R., Chiosi, C., Bressan, A., & Fagotto, F. 1996, *â*, 311, 361
- Whitmore, B. C., Miller, B. W., Schweizer, F., & Fall, S. M. 1997, AJ, 114, 1797
- Worthey, G. 1994, ApJS, 95, 107
- Worthey, G., Dorman, B., & Jones, L. 1996, AJ, 112, 948
- Worthey, G., Faber, S. M., & Gonzalez, J. J. 1992, ApJ, 398, 69

TABLE 1
MID-UV^a AND OPTICAL^b SPECTRAL INDICES

Index	Absorption Band (Å)	Continuum Bands (Å)
Fe2402	2382-2422	2285-2325 2432-2458
Bl2538	2520-2556	2432-2458 2562-2588
Fe2609	2596-2622	2562-2588 2647-2673
Mg2800	2784-2814	2762-2782 2818-2838
Mg2852	2839-2865	2818-2838 2906-2936
MgWide	2670-2870	2470-2670 2930-3130
Fe3000	2965-3025	2906-2936 3031-3051
H β	4848-4877	4828-4848 4877-4892
Mg ₂	5154-5197	4895-4958 5301-5366

^aFanelli et al. 1990

^bFaber et al. 1985

TABLE 2
GLOBULAR CLUSTER DATA^a

Cluster ^b	Z	EW Å	C_{2466} $\frac{\log(F)}{\log(F_{2646})}$	C_{2959} $\frac{\log(F)}{\log(F_{2646})}$	C_{3122} $\frac{\log(F)}{\log(F_{2646})}$	Bl2538 mag	S2850 $\frac{\Delta mag}{1000A}$
G2b	0.006	28.6	0.53	1.55	2.07	0.593	-1.65
G47Tuc	0.004	34.2	0.46	1.46	2.06	0.759	-1.60
G3b	0.0011	20.7	0.63	1.27	1.33	0.396	-0.68
G3r	0.0010	23.4	0.66	1.24	1.42	0.496	-0.80
G4b	0.0007	12.7	0.80	1.12	1.24	0.224	-0.48
G4r	0.0006	21.6	0.68	1.23	1.30	0.416	-0.63
G5	0.0002	9.1	0.85	1.18	1.27	0.156	-0.55

^aEW and continuum points C_{2466} , C_{2959} , C_{3122} were taken from Bonatto et al. 1995

^bNames of composite globular cluster spectra; r = red, b = blue

TABLE 3
FOS OBSERVATIONS

Galaxy	Grating	Exposure Time
NGC1399	G130H	10453s
	G190H	5284
	G270H	3542
NGC3610	G130H	10453
	G190H	5836
	G270H	3531

TABLE 4
GALAXY DATA^a

Galaxy	B12538	B12538 corrected	S2850	S2850 corrected	Mg ₂
M 32	0.45	-	-2.92	-	0.194
M 31	0.34	0.49	-2.29	-2.73	0.286
NGC 1399	0.07	0.30	-1.02	-1.65	0.312
NGC 3610 ^b	0.30	0.38	-2.59	-2.73	0.271 ^c
NGC 1399 ^b	0.08	0.23	-0.80	-2.04	0.357 ^d

^aUV data extracted from IUE database by D. Calzetti; optical data from Kinney et al. 1996

^bFOS data, see section 4

^cWorthey et al. 1992

^dMg₂ value of nucleus from Burstein et al. 1988

TABLE 5
12 GYR BIMODAL METALLICITY MODELS

% Z=0.0004 mass	Z=0.0004 / Z=0.02 model % Z=0.0004 mid-UV flux	Z=0.0004 / Z=0.05 model % Z=0.0004 mid-UV flux
0.5%	11%	35%
1%	19%	52%
5%	55%	85%
10%	72%	92%
15%	81%	95%

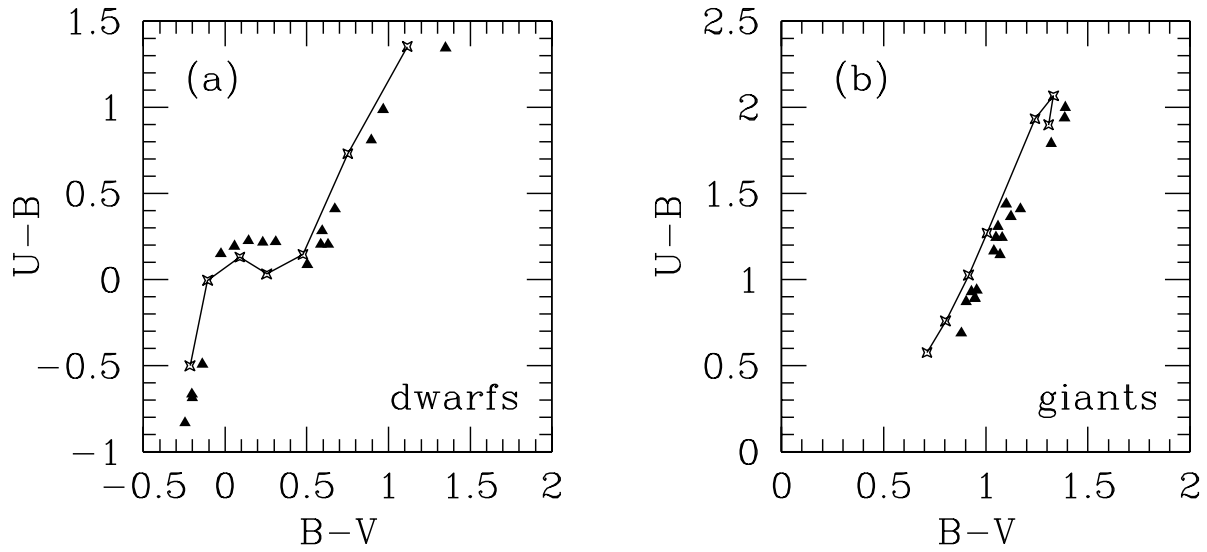


Fig. 1.— (a,b) $(U - B)$ v. $(B - V)$ for Kurucz solar metallicity dwarf (a) and giant (b) stellar atmospheres (crosses connected by lines) against the Gunn-Stryker stars (filled triangles).

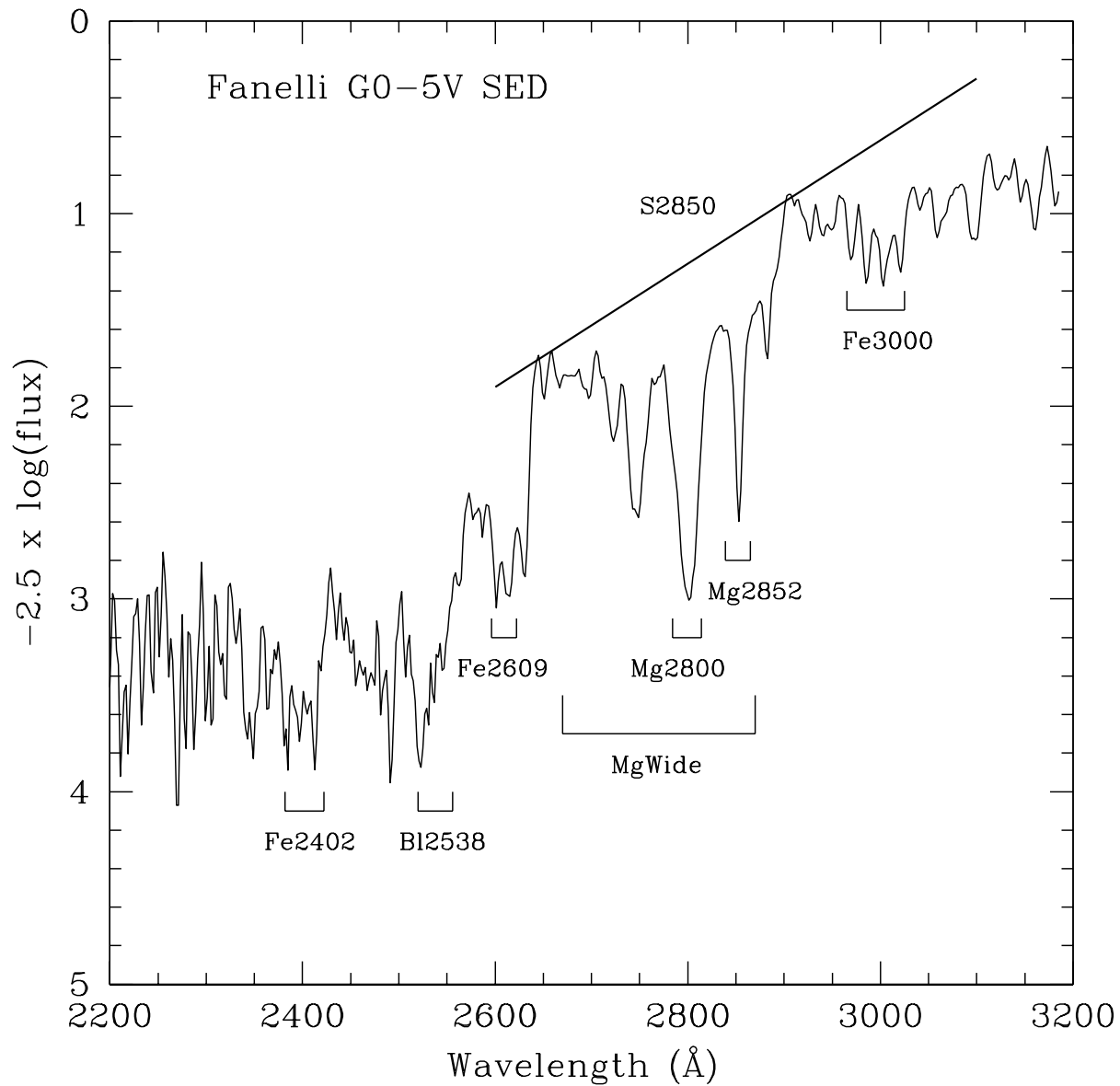


Fig. 2.— The Fanelli composite IUE spectra for G0-5V stars is shown with the mid-UV spectral indices and $S2850$ identified (Table 1). $S2850$ is defined as the continuum slope between 2600 \AA and 3100 \AA , excluding the absorption features.

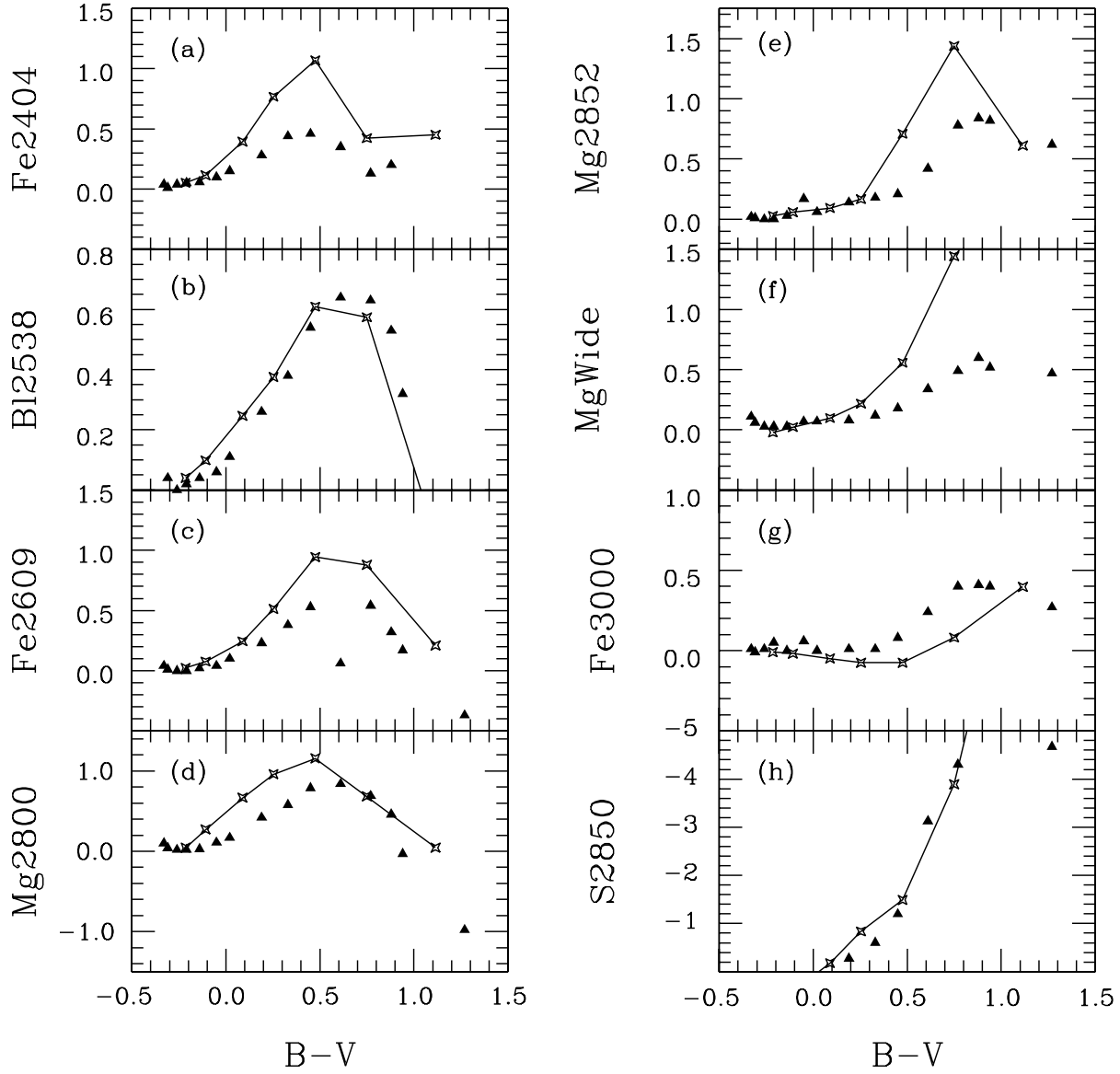


Fig. 3.— (a-h) The mid-UV absorption lines and continuum values for Kurucz model $Z=0.02$ dwarfs (crosses connected by lines) are plotted against $(B-V)$ with observed values for Fanelli IUE composite dwarf spectra (triangles). Note that only the BI2538 (b) and S2850 (h) are well modeled by the Kurucz atmospheres.

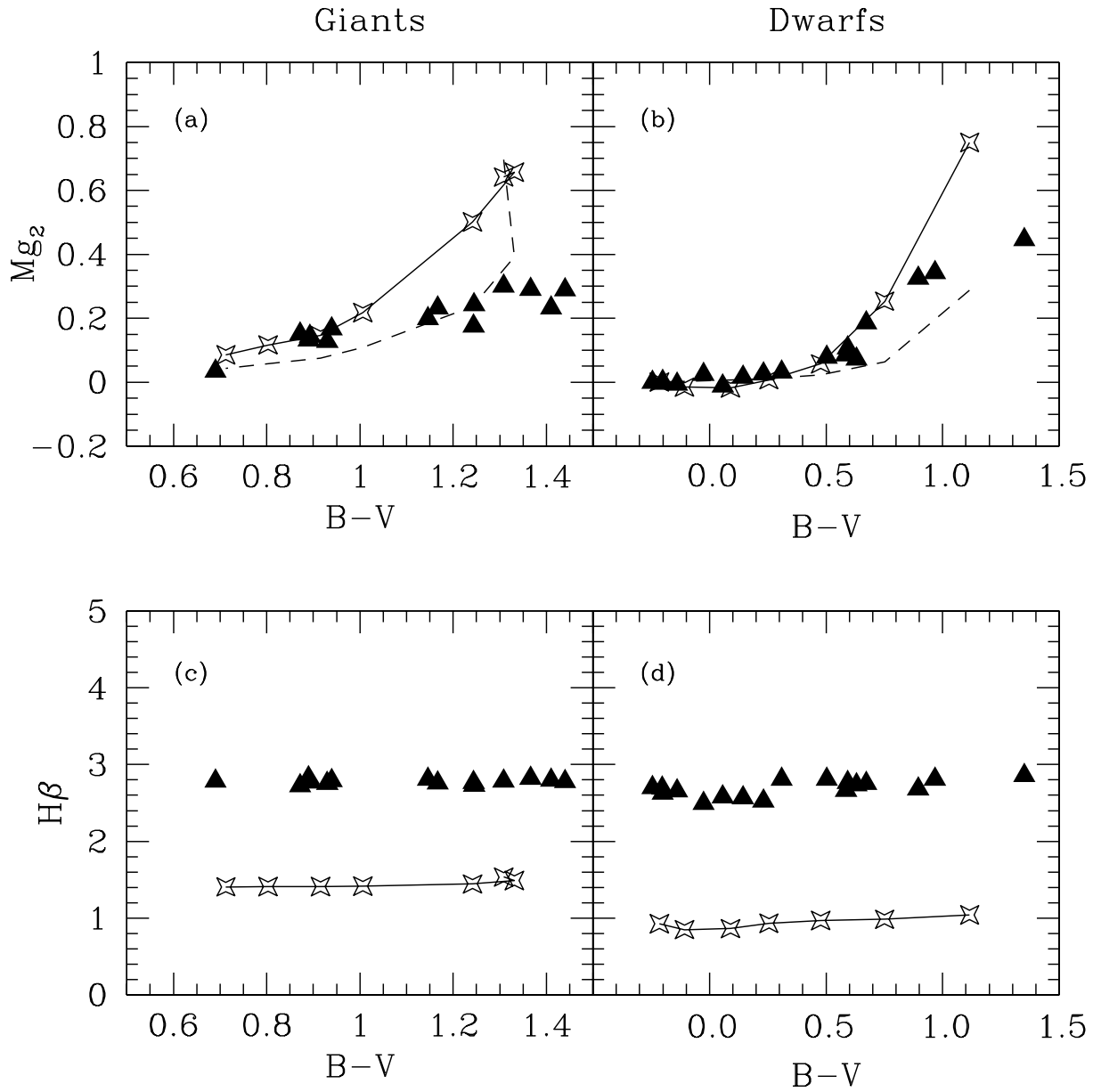


Fig. 4.— (a,b)The optical absorption feature Mg_2 for the Kurucz model $Z=0.02$ dwarfs and giants (crosses connected by lines) are plotted against $(B - V)$ with observed values for dwarfs and giants taken from the Gunn-Stryker catalog (triangles). (c,d) Same for $H\beta$.

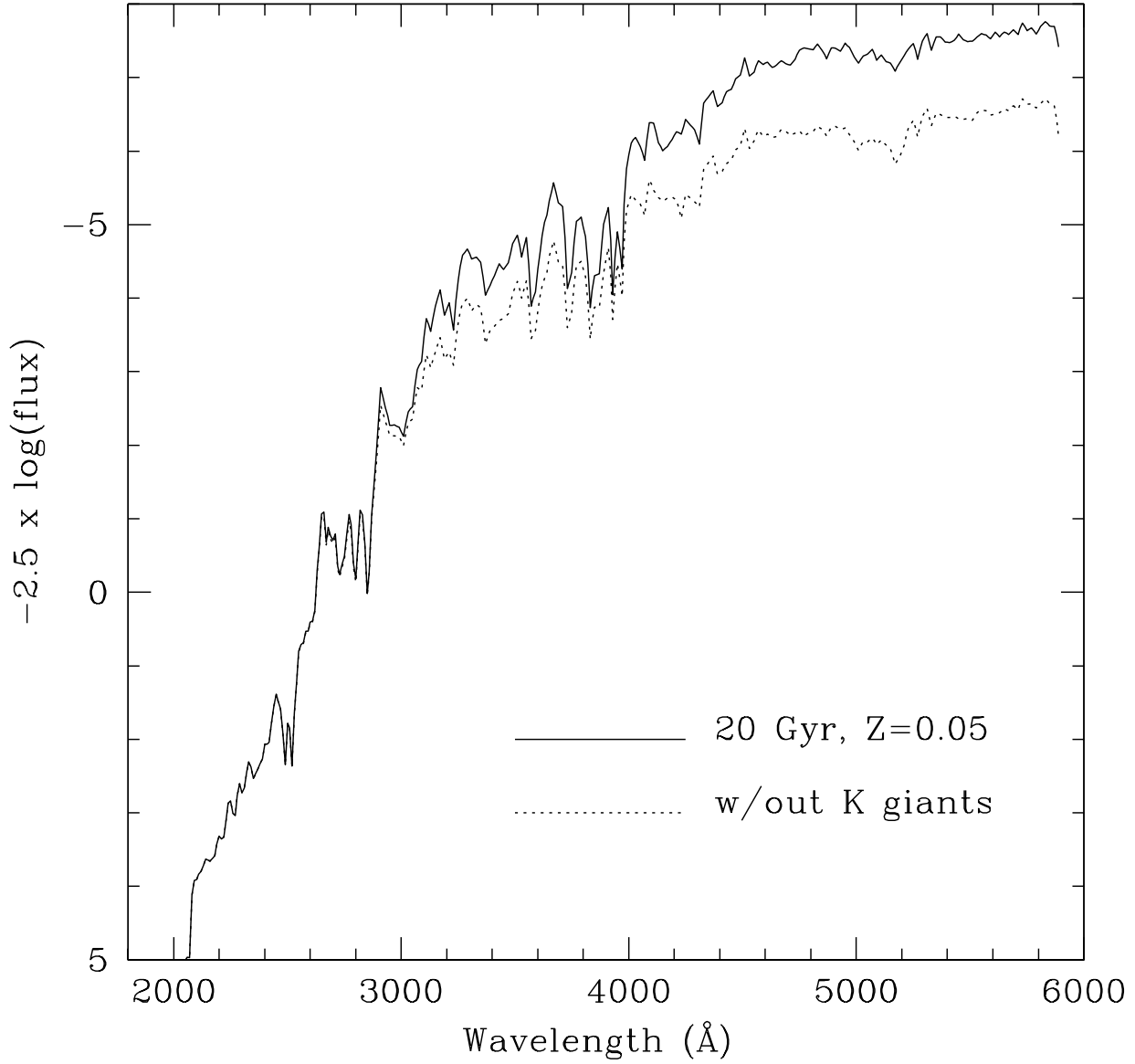


Fig. 5.— 20 Gyr, $Z=0.05$ SED created with cool giants (solid line) and without cool giants (dotted line). Note that the cool giants contribute very little light to 1800 - 3200 Å but do dominate the Mg_2 at ~ 5170 Å.

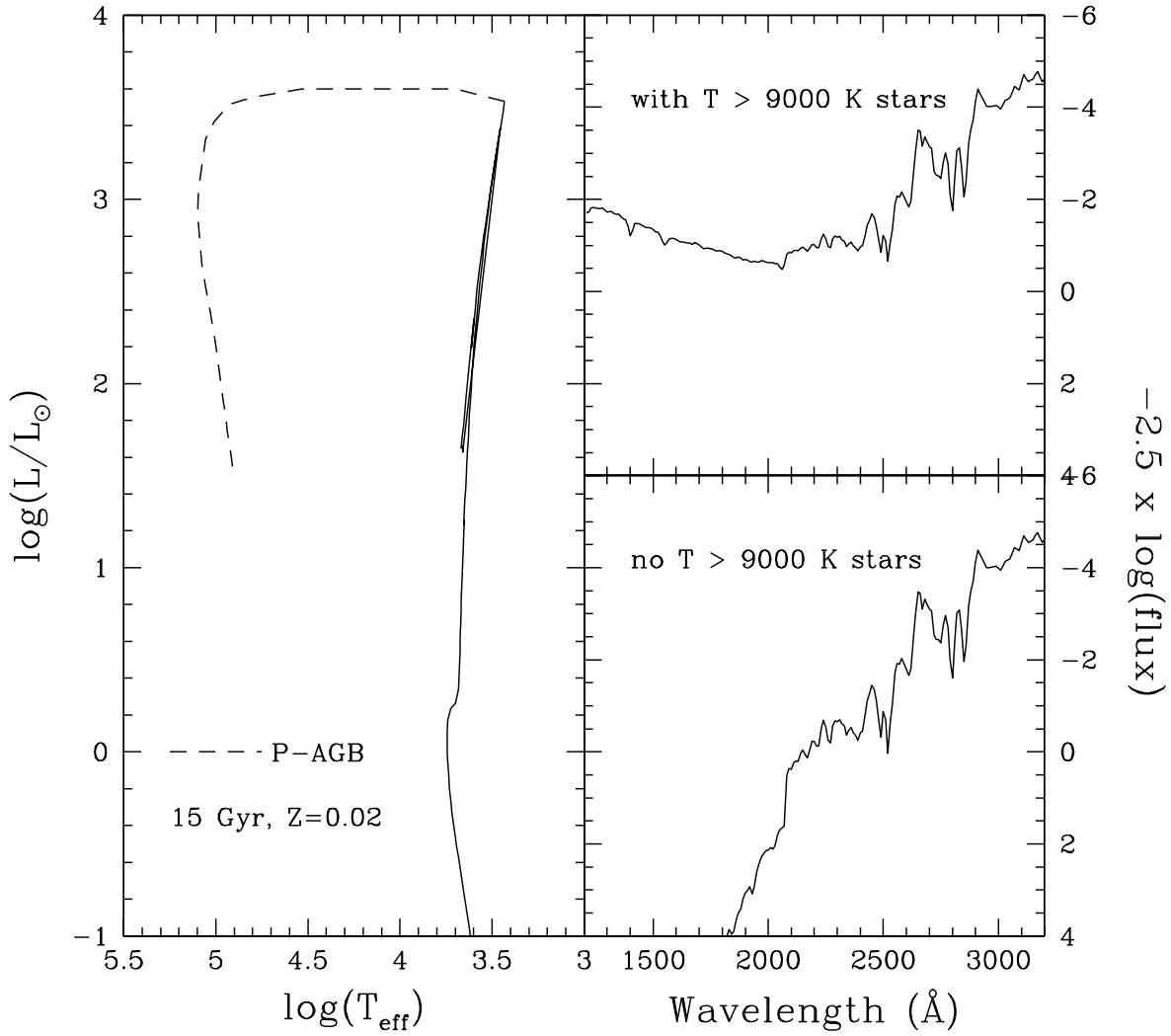


Fig. 6.— The left hand panel show the Padova isochrone for a 15 Gyr, solar population. The dashed line is the P-AGB. The right-hand panels show the UV region for the SED (Wavelength v. $-2.5 \times \log(\text{flux})$) calculated with and without stars hotter than 9000 K. Note that the far-UV (wavelength $\geq 2000 \text{\AA}$) is dominated by flux from the P-AGB.

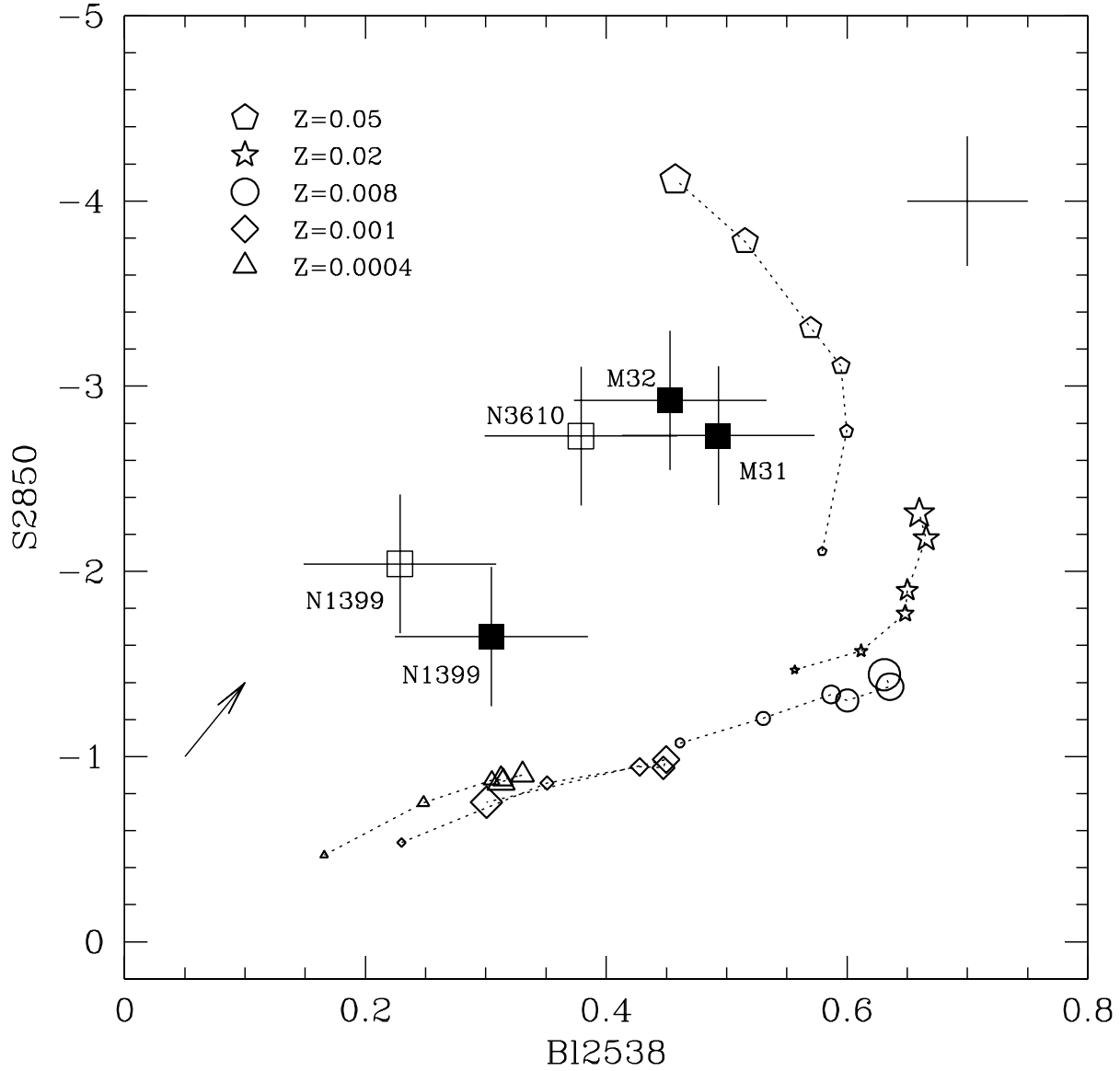


Fig. 7.— B12538 index v. S_{2850} for the single age (3, 7, 10, 12, 15, and 20 Gyr), single metallicity ($Z=0.0004, 0.001, 0.008, 0.02,$ and 0.05) SEDs with *no hot stellar component*. Different metallicities have different symbols defined by the legend and increasing age models are represented by increasingly larger symbols with the smallest symbol = 3 Gyr and the largest symbol = 20 Gyr. The galaxies are plotted as squares (open for FOS, closed for IUE). The uncertainty for the model SEDs is given by the error bar in the upper right corner. The effect of reddening for $A_B = 0.5$ is shown by the arrow in the lower left.

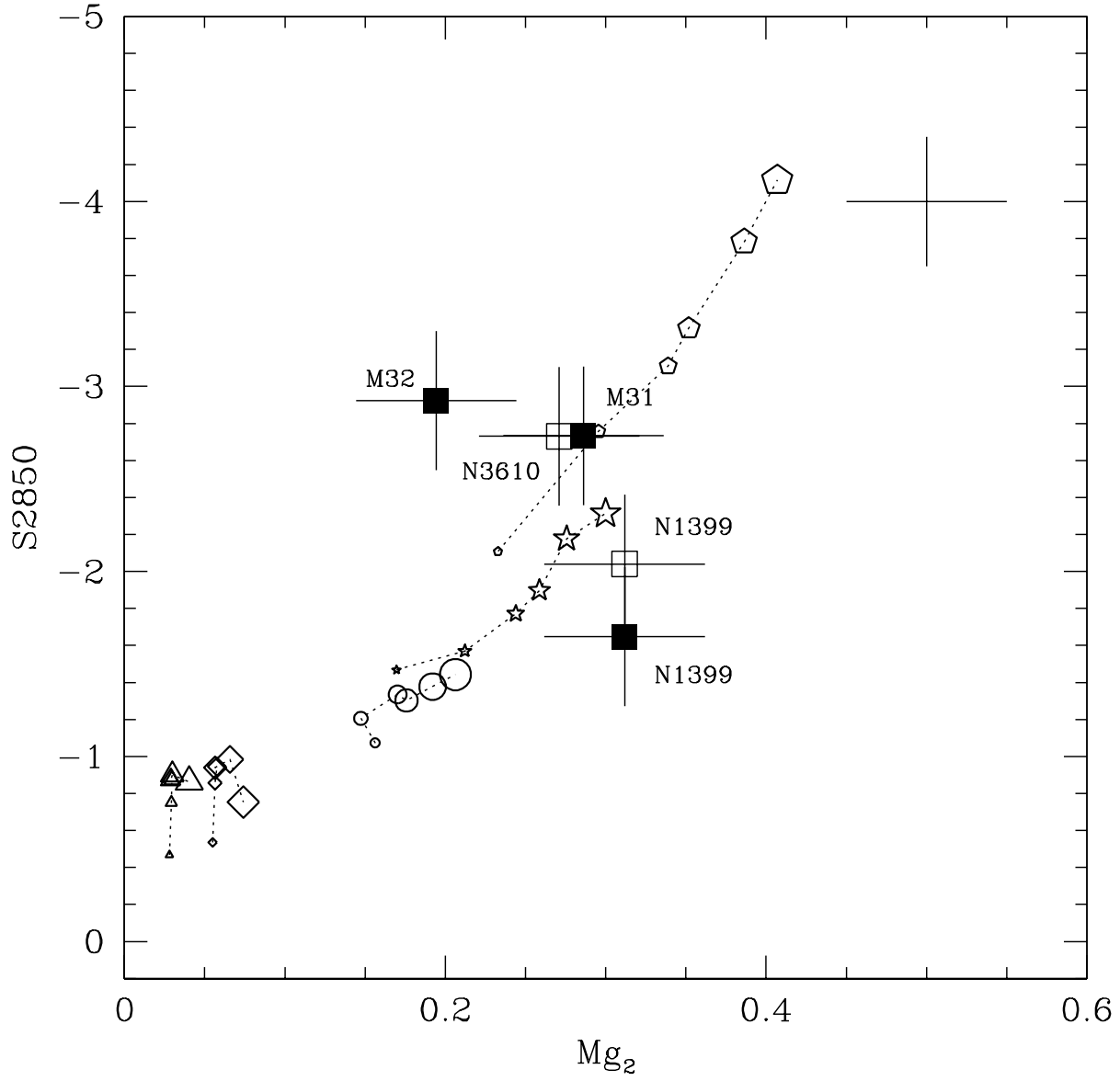


Fig. 8.— S_{2850} v. Mg_2 for single age, single metallicity models with *no hot stellar component*. Symbols are the same as for Figure 7.

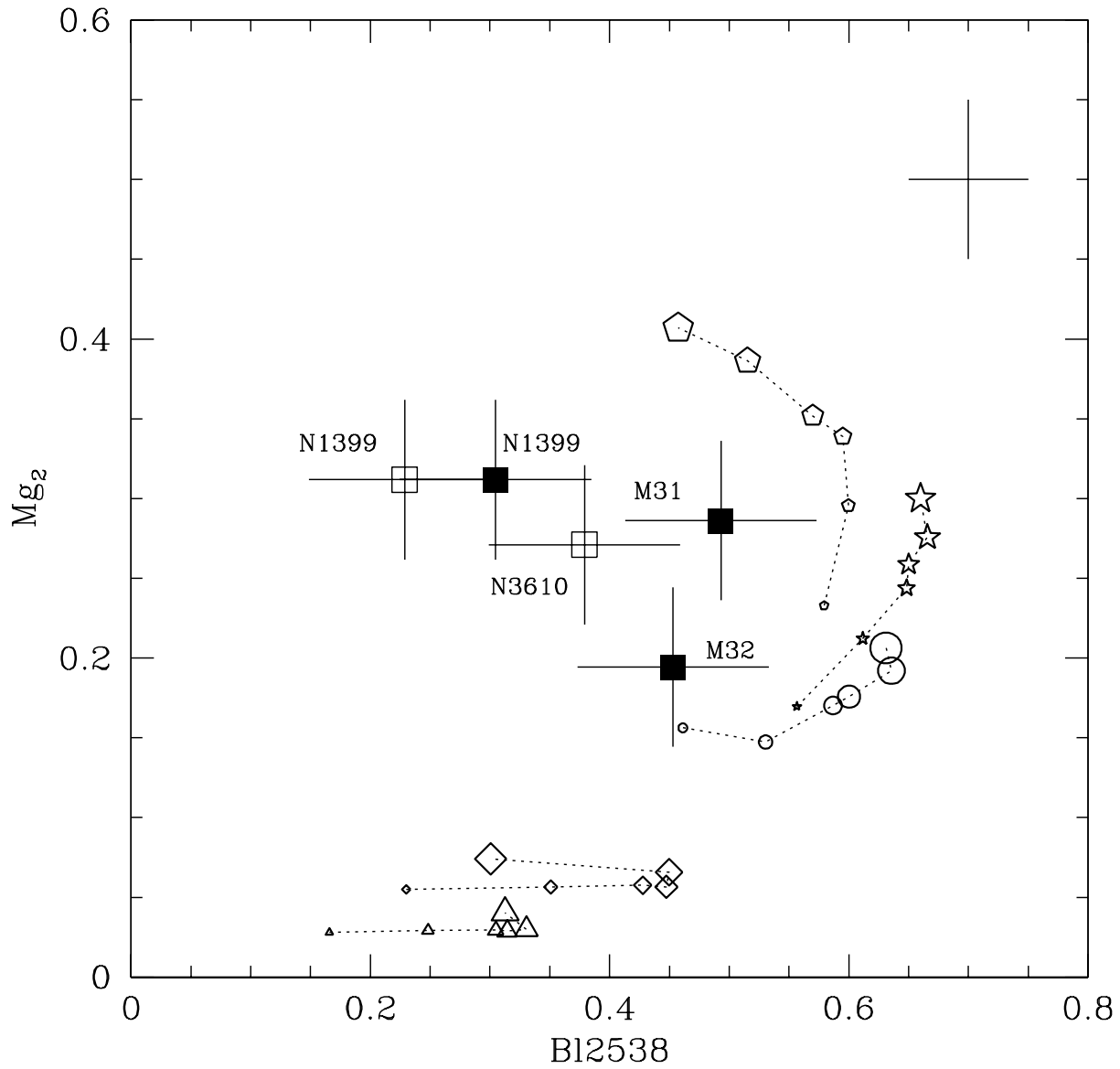


Fig. 9.— B12538 v. Mg₂ for single age, single metallicity models with *no hot stellar component*. Symbols are the same as for Figure 7.

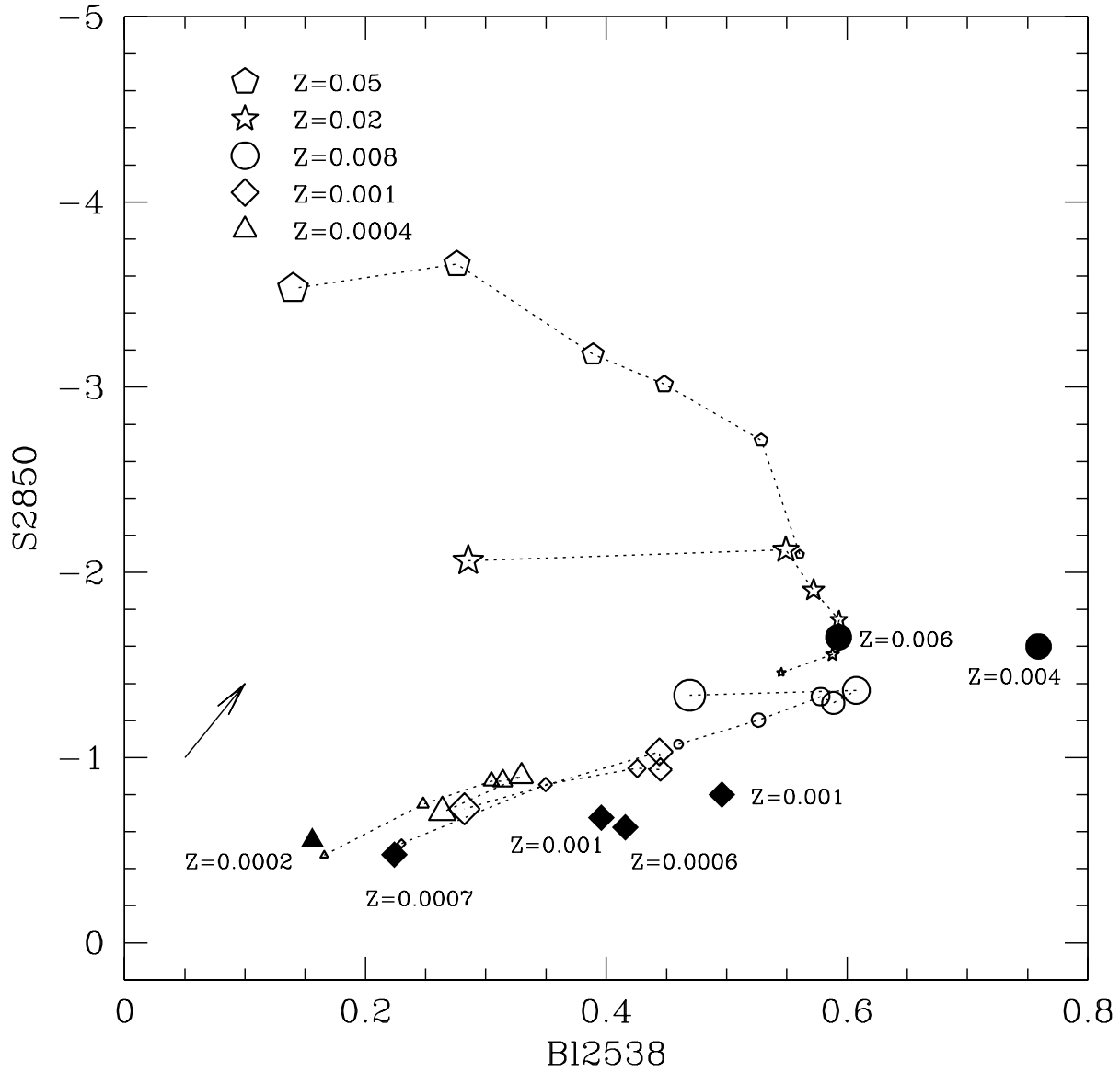


Fig. 10.— B12538 v. S2850 for single age, single metallicity models computed with the original isochrone and including the hot HB and post HB stars. The composite IUE globular cluster values (Table 2, Bonatto et al 1995) are plotted as filled symbols, with the shape of the symbol corresponding to cluster metallicity.

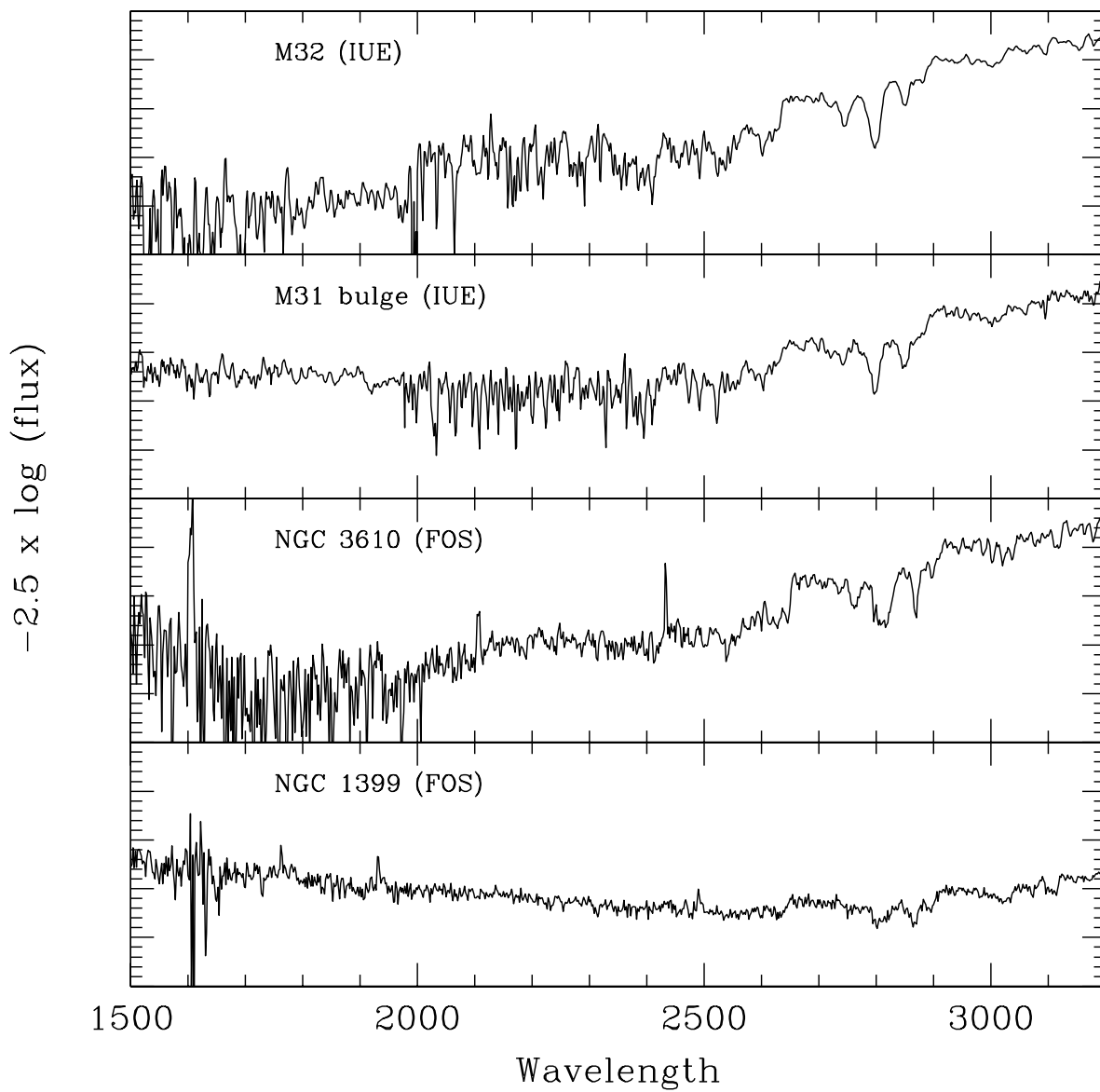


Fig. 11.— The mid-UV spectra of M32, the bulge of M31, NGC 3610, and NGC 1399. The FOS data has been binned to 2 Å resolution. Each large tickmark corresponds to 1 magnitude.

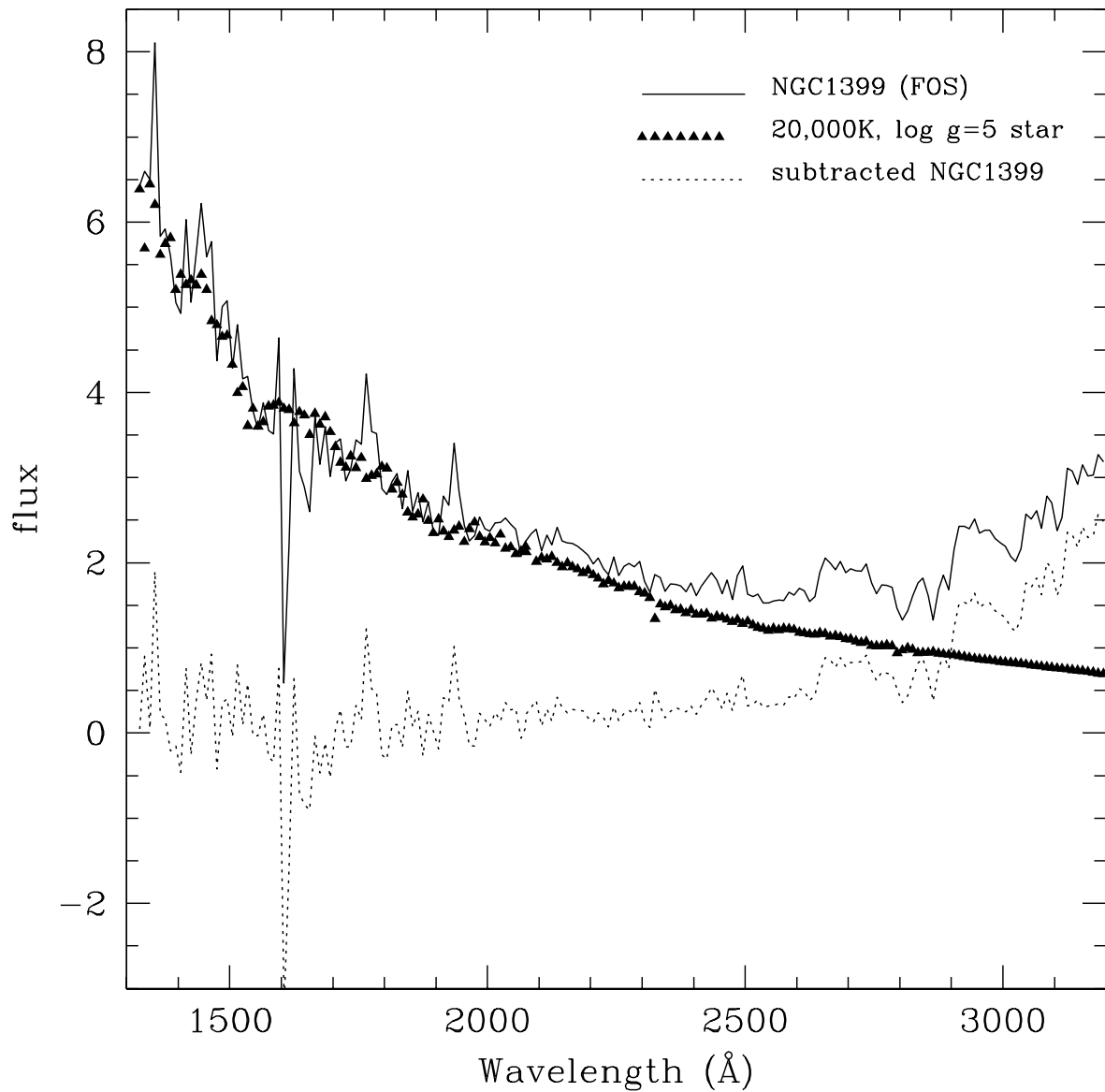


Fig. 12.— The FOS spectra of NGC 1399 is plotted (solid line) with the 20,000 K, $\log g = 5.0$ Kurucz atmosphere fitted to NGC 1399 far UV flux (triangles). The far UV subtracted NGC 1399 spectra is given by the dashed line.

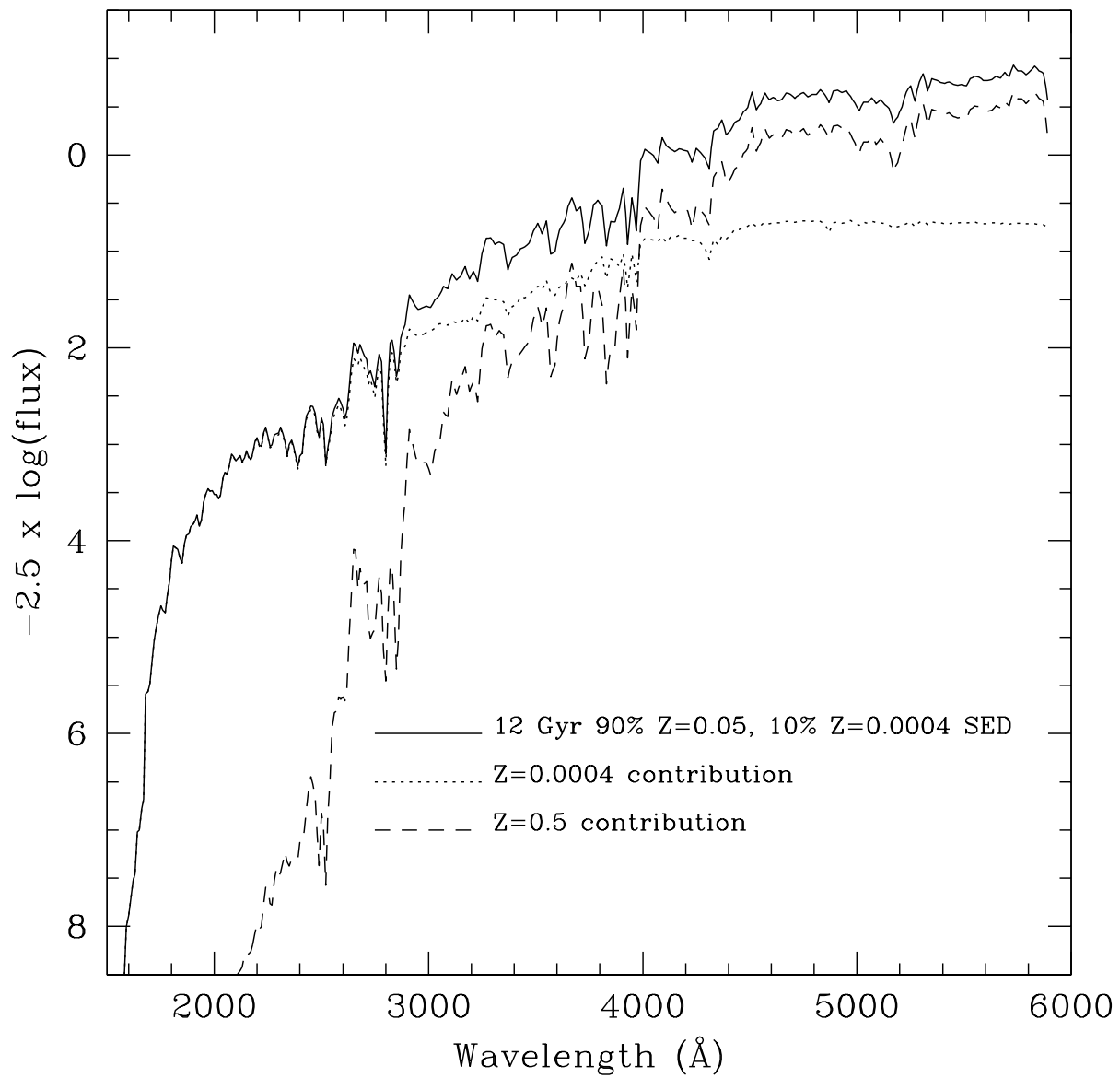
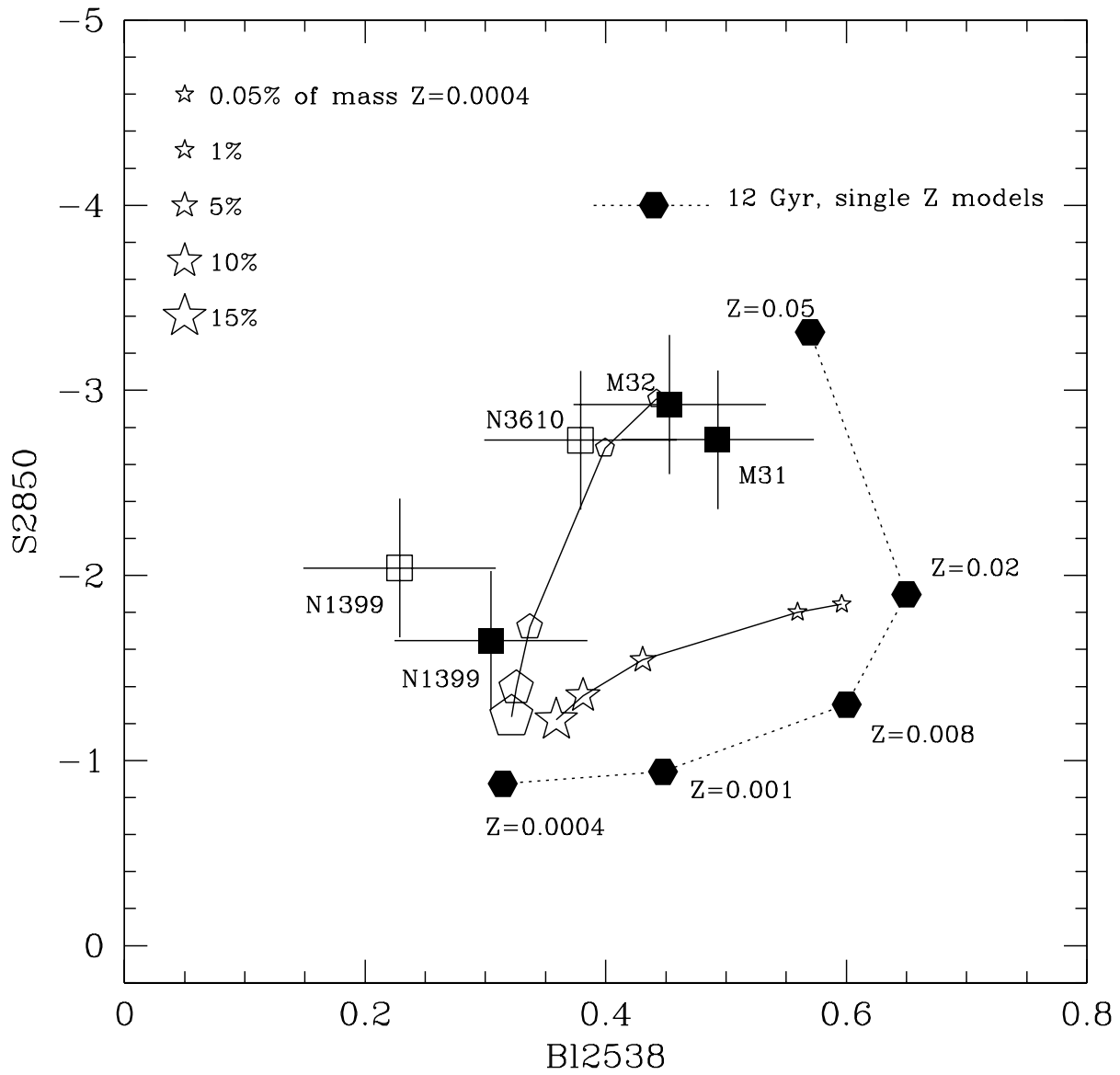
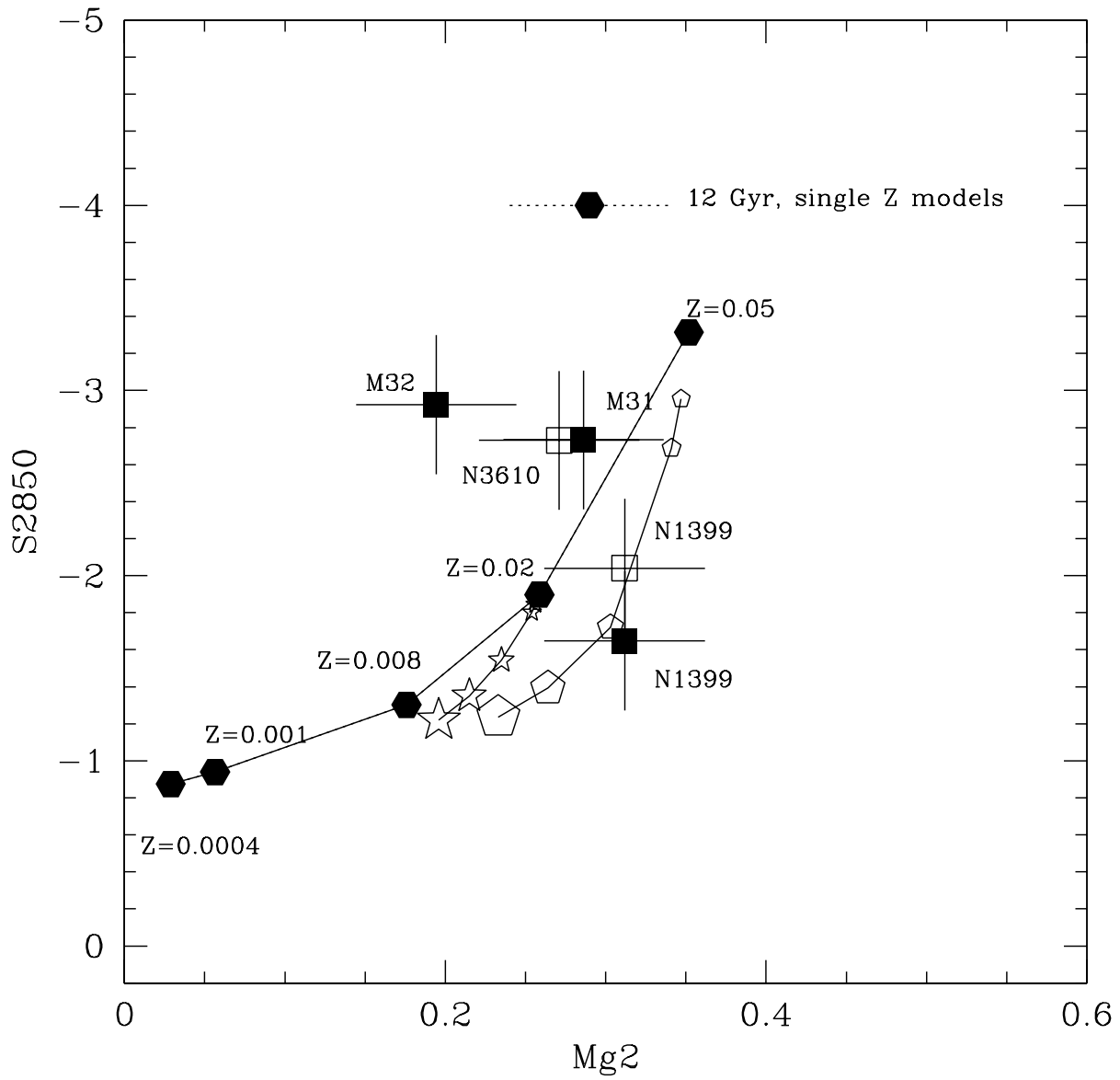


Fig. 13.— Bi-modal metallicity 12 Gyr SED (solid line) where 10 % of mass is from a $Z=0.0004$ population (dot-dashed line) and 90 % from a $Z=0.05$ population (dashed line).





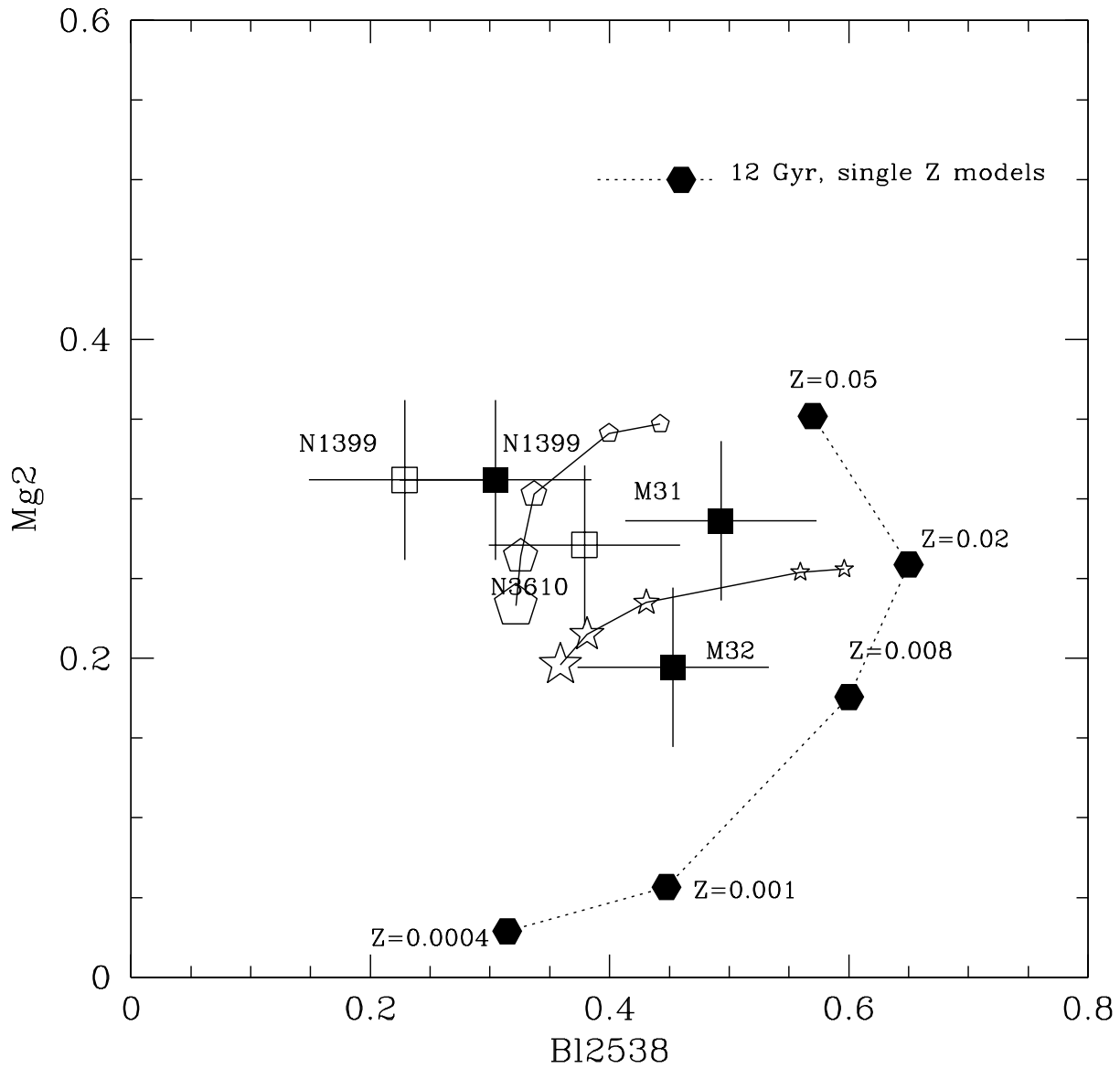


Fig. 14.— (a-c) $S2850 \text{ v Bl2538}$, $S2850 \text{ v Mg}_2$, $\text{Mg}_2 \text{ v Bl2538}$; Bi-modal metallicity models for 12Gyr, $Z=0.05/0.0004$ models are represented by the pentagons, and the $Z=0.02/0.0004$ models are represented by the stars. The models given have 0.5%, 1%, 5%, 10% and 15% of total mass from the metal-poor subpopulation. For comparison, the 12 Gyr single abundance models are given as well.

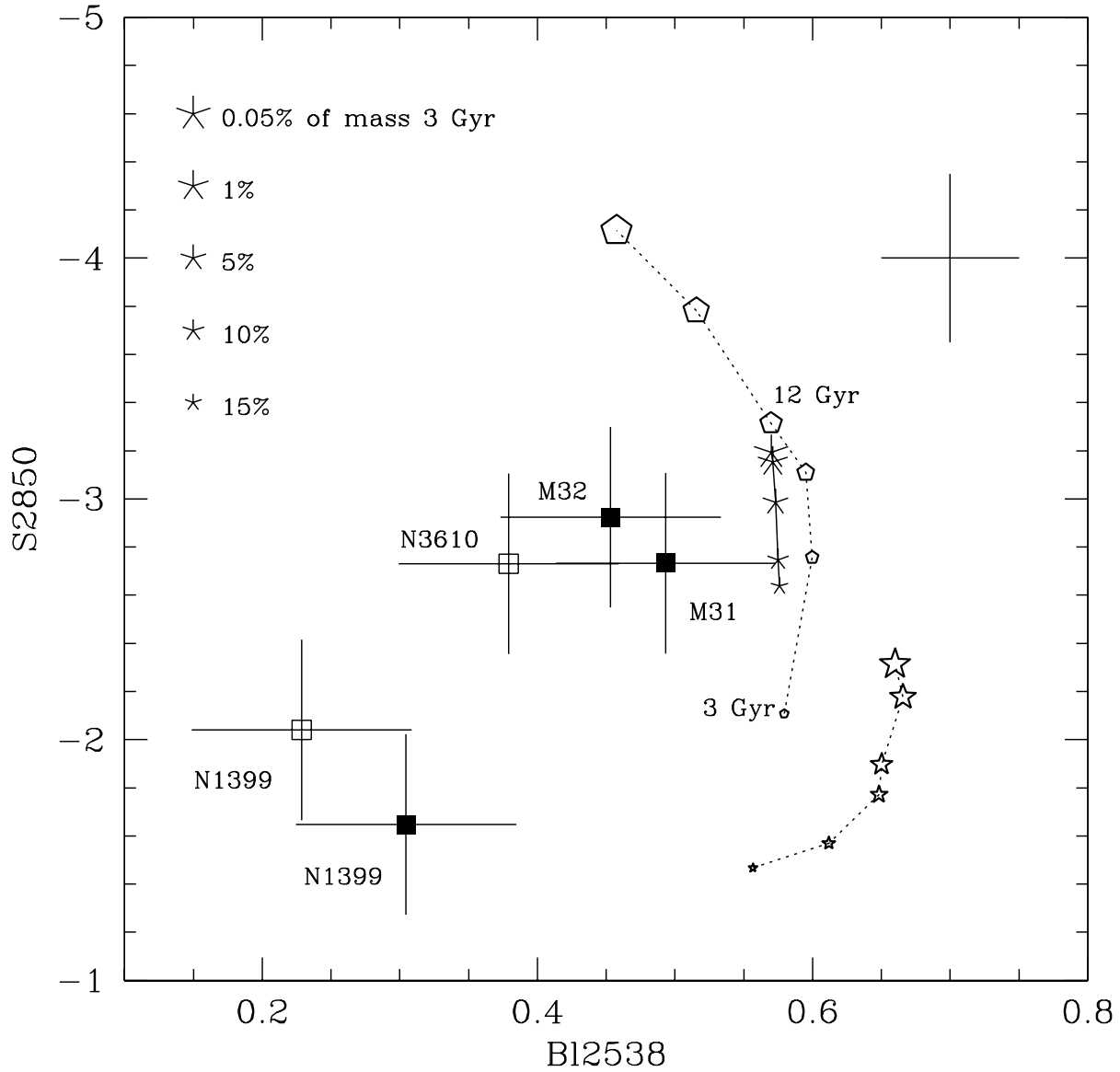


Fig. 15.— Composite 3 Gyr/12 Gyr $Z=0.05$ models (asterisks) are computed for increasing mass of the young 3 Gyr sub-population. The single age $Z=0.05$ (pentagons) and $Z=0.02$ (stars) are shown as well for comparison. Note that M 32 is not matched by any of the composite models.

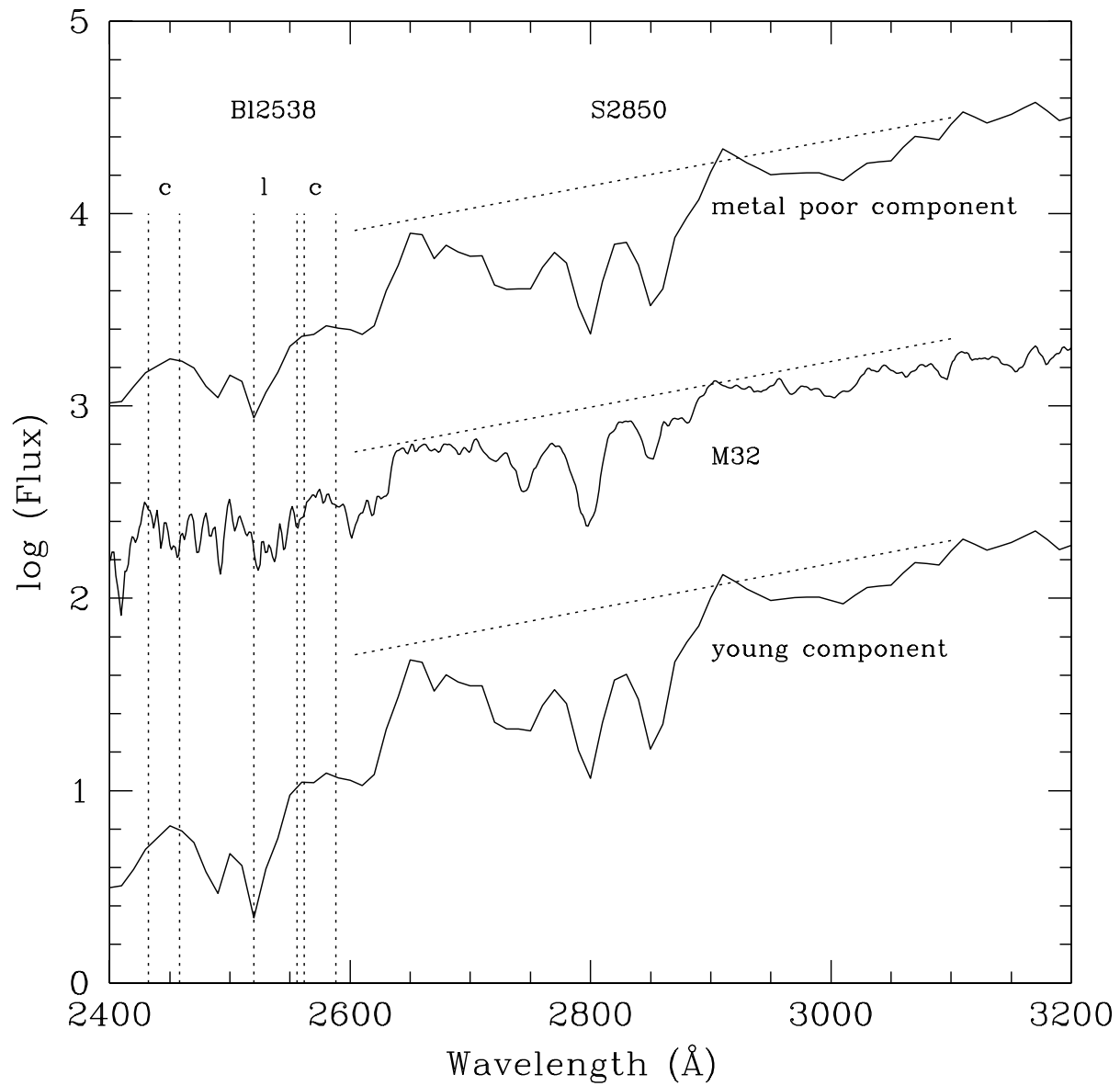


Fig. 16.— M 32 mid-UV spectra is compared to the 0.5 % $Z=0.0004$ / 99.5% $Z=0.05$ 12 Gyr and the 5% 3 Gyr / 95% 12 Gyr $Z=0.05$ models. See Fig. 14a and Fig 15 for *BI2538* and *S2850*.